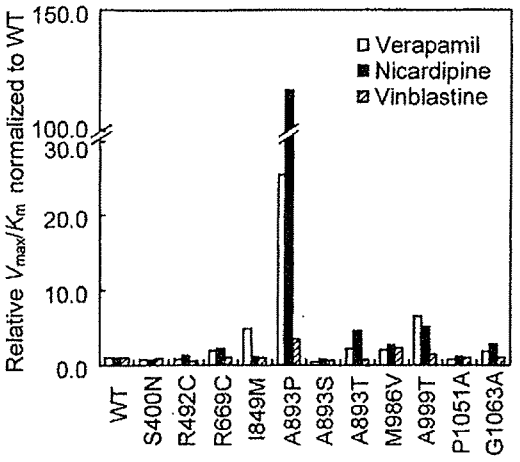

FIGURE 4: V_{max}/K_m values of ABCB1 WT and variants observed for verapamil, nicardipine, and vinblastine. Drug-stimulated ATPase activity of the ABCB1 WT and SNP variants was measured as described in Experimental Procedures. Sf9 plasma membranes (2 μg of protein) expressing ABCB1 were incubated with 2 mM ATP and a drug at different concentrations at 37 °C for 30 min. After the incubation, the amount of liberated phosphate was measured. On the basis of Lineweaver–Burk plots, V_{max} and K_m values were determined, and the relative V_{max}/K_m values of SNP variants were calculated by normalizing to the WT. (The relative V_{max}/K_m value of WT = 1.)

exhibited a markedly high ATPase activity toward verapamil (Figure 3, upper panel). Similar saturation kinetics was also observed with nicardipine, another vasodilator. Tables 2 and 3 summarize the kinetic parameter K_m and V_{max} values for those variants toward verapamil and nicardipine, respectively. Accordingly, the value of V_{max}/K_m has been calculated for each variant.

Figure 4 graphically demonstrates the relative V_{max}/K_m values of SNP variants toward verapamil, nicardipine, and vinblastine. In this graph, the relative V_{max}/K_m values of SNP variants were normalized to those of WT. Among those SNP variants, the A893P variant exhibited a very high value (118-fold) of the relative V_{max}/K_m toward nicardipine (Figure 4). On the other hand, the V_{max}/K_m value of the A893P variant toward vinblastine was only 3-fold higher than that of WT (Figure 4). In contrast, the A893S variant exhibited the lowest value of V_{max}/K_m toward those substrates (Figure 4). These results suggest that nonsynonymous SNPs affect the substrate specificity of ABCB1 as referred to the drug-stimulated ATPase activity.

Profiling of Drug-Stimulated ATPase of ABCB1 WT, A893P, A893S, and A893T. To gain more insight into the effect of nonsynonymous polymorphisms on the substrate specificity of ABCB1, we first tested the substrate specificity of ABCB1 WT and SNP variants by measuring their drug-stimulated ATPase activity toward a total of 41 structurally unrelated test compounds. In this measurement, the concentration of those test compounds was equally 10 μM in the reaction mixture, since this concentration was optimal to obtain the drug-stimulated ATPase activity profile of ABCB1 toward a variety of test compounds. At higher concentrations, certain hydrophobic compounds were not completely dissolved. The test compounds are classified into seven groups, i.e., A, neurotransmitters; B, vasodilators, C, steroids; D, potassium channel modulators; D, nonsteroidal antiinflammatory drugs (NSAIDs); F, anticancer drugs; and G, miscellaneous.

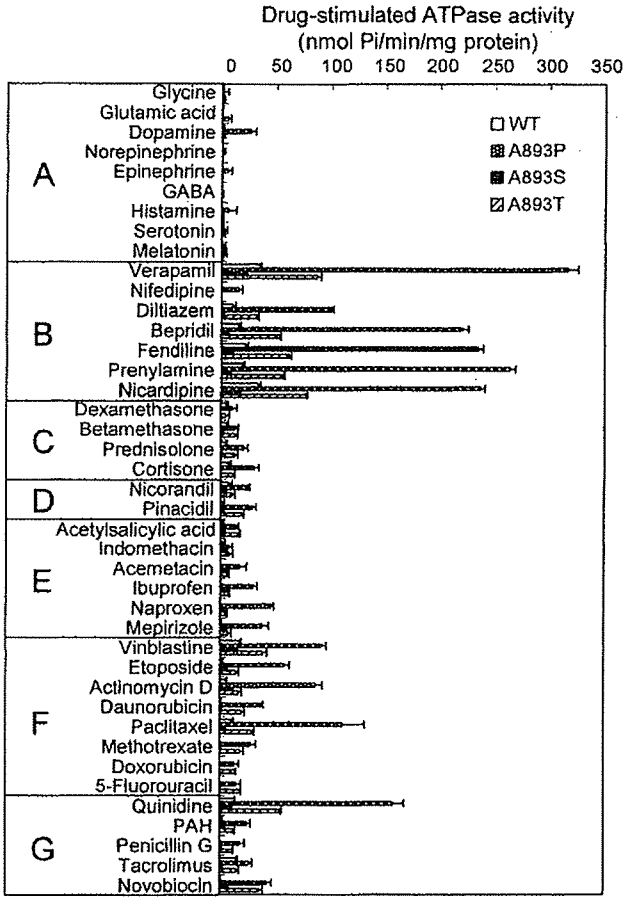

FIGURE 5: Effect of test compounds on the ATPase activity of ABCB1 WT, A893P, A893S, and A893T. The ATPase activity was measured in the presence of 10 μM test compound as described in Experimental Procedures. All activities are expressed as mean values ± SD (n = 4). (A) neurotransmitters; (B) vasodilators, (C) steroids; (D) potassium channel modulators; (E) nonsteroidal antiinflammatory drugs (NSAIDs); (F) anticancer drugs; (G) miscellaneous.

Figure 5 demonstrates typical results on the drug-stimulated ATPase activity profiles of ABCB1 WT and A893S, A893T, and A893P variants. Among the 41 different therapeutic drugs and compounds tested here, significantly high drug-stimulated ATPase activities were observed in vasodilators, such as verapamil, diltiazem, bepridil, fendiline, prenylamine, and nicardipine, for ABCB1 WT, A893P, A893S, and A893T. In particular, A893P and A893T variants exhibited higher drug-stimulated ATPase activities toward those vasodilators than did ABCB1 WT. Moderate drug-stimulated ATPase activities were observed toward several anticancer drugs, such as vinblastine, etoposide, actinomycin D, and paclitaxel. In those anticancer drugs also, A893P exhibited the highest value of drug-stimulated ATPase activity among ABCB1 WT and SNP variants.

Profiling of Drug-Stimulated ATPase and QSAR Analysis To Evaluate the Substrate Specificity of SNP Variants. The same profiling of drug-stimulated ATPase activities was performed for the other SNP variants to compare with those of ABCB1 WT as well as A893P, A893S, and A893T variants (data not shown). As described above, we have measured the drug-stimulated ATPase activity of all of the prepared SNP variants as well as the WT toward a total of 41 test compounds (10 μM for each in the reaction mixture)

Table 4: Descriptors and Chemical Fragmentation Codes (CFC) Closely Correlated with the ATPase Activity of ABCB1 WT and Variant Proteins[a]

descriptor	CFC	score	description
M532	M532	1.0	two carbocyclic systems with at least one aromatic ring
M132	M132	1.0	ring-linking groups containing 1C atom
C-CHN-BT			one or more carbon chains bonded to ring C, V, C=V, C·V, C=U, C·U, or U applicable
	M281	1.0	one
	M282	2.0	two
	M283	3.0	three or more
ESTR			ester (thioester) group bonded to heterocyclic C via >C=O (>C=S)
	J211	1.0	one
	J212	2.0	two or more
OH-Ar			−OH group bonded to aromatic C
	H441	1.0	one
	H442	2.0	two
	H443	3.0	three
	H444	4.0	four or more
R-CC			carbocyclic systems with at least one aromatic ring
	M531	1.0	one
	M532	2.0	two
	M533	3.0	three or more
RT			ring tertiary N (amine and non-amine)
	H201	1.0	one amine
	H202	2.0	two amines
	H203	3.0	three or more amines
	H211	1.0	one non-amine
	H212	2.0	two non-amines
	H213	3.0	three or more non-amines
-O-Ar			ether with −O− bonded to aromatic C
	H541	1.0	one
	H542	2.0	two
	H543	3.0	three or more
D012	D012	1.0	one atom of fused heterocyclic ring bears substituent(s); atom is not at or adjacent (atom is beta) to ring fusion
G010	G010	1.0	one substituted C atom in an unfused aromatic ring
H100	H100	1.0	one primary amine
H181	H181	1.0	one amine bonded to aliphatic C
H421	H421	1.0	one −OH group bonded to heterocyclic C
H521	H521	1.0	one ether with −O− bonded to heterocyclic C
M113	M113	1.0	benzene linked to other ring (non-benzene or non-aryl ring) by a single or double bond
M232	M232	1.0	carbon chain containing secondary branching
M280	M280	1.0	no 0-valent or monovalent carbon chains present
M313	M313	1.0	3C atoms in polyvalent chain
M332	M332	1.0	straight carbon chain with none of the groups $-CH_3$, $-C{=}CH_2$, or −C·CH
M370	M370	1.0	carbon chain bonded to a ring C and (U and/or C=U and/or C·U) but not to V, C=V, or C·V
M372	M372	1.0	bonded to ring −C and C=U and/or C·U only
M392	M392	1.0	multipliers for codes M350 to M383 (polyvalent carbon chain attachments) twice
M531	M531	1.0	one carbocyclic system with at least one aromatic ring
M540	M540	1.0	no alicyclic systems
H7	H7	1.0	absence of olefinic/acetylinic groups
H8	H8	1.0	absence of ether or hydroxy
L1	L1	1.0	absence of −C≡N, −N≡C
L9	L9	1.0	absence of functional groups in rings

[a] U represents atoms such as O, S, Se, Te, or N. V represents atoms other than C, H, O, S, Se, Te, or N.

by using our high-speed screening system (*32*). On the basis of the drug-stimulated ATPase profiling data, we performed QSAR analysis to elucidate the substrate specificity of the ABCB1 WT and SNP variants. We used the CFCs to describe the chemical structures of a variety of substrates and nonsubstrates for ABCB1. The Markush TOPFRAG was used to generate CFCs for each compound tested. Table 4 provides explanations for descriptors and CFCs generated in the analysis, where some descriptors (e.g., C-CHN-BT, ESTR, OH-Ar, RT, and -O-Ar) represent multiple CFCs. In this way, however, steroids (group C) and actinomycin D (group F) were excluded from this analysis, because the Markush TOPFRAG program does not have an algorithm to generate CFCs for those compounds.

The multiple linear regression analysis was then carried out to obtain a relationship between the drug-stimulated ATPase activity and the CFCs thus generated. Thereby, we could identify one set of descriptors and/or CFCs related to the substrate specificity of each of the ABCB1 WT and SNP variants. The best-fitting models were created by multiple linear regression analysis, where the predicted activity of the drug-stimulated ATPase of ABCB1 was described as a linear combination of CFCs weighted by the corresponding coefficient, $C(i)$ (see Experimental Procedures). Figure 6 demonstrates the relationships between the drug-stimulated ATPase activities observed with 10 μM test compounds and the predicted ATPase activities for ABCB1 WT, A893P, A893S, and A893T. As clearly shown in this figure, the prediction of drug-stimulated ATPase activity was well correlated with the observed values.

We carried out the same QSAR analysis for all of the variants tested in this study, and Table 5 summarizes the

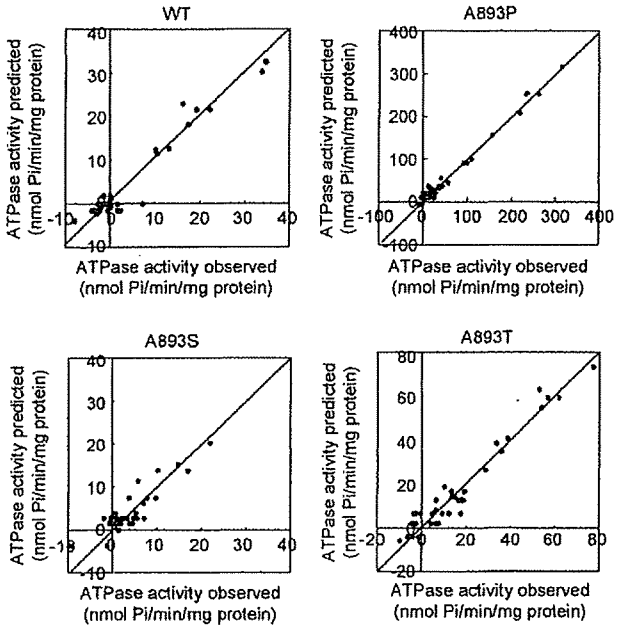

FIGURE 6: Relationships between observed and predicted ATPase activities for ABCB1 WT, A893P, A893S, and A893T. The actual ATP activities were observed with 10 μM test compounds as shown in Figure 5. The predicted ATPase activities were calculated by multiple linear regression analysis performed for ABCB1 WT, A893P, A893S, and A893T.

contents of these multiple linear regression analysis models. The QSAR analysis revealed that the structural components represented by the CFCs of M532 and M132 as well as the descriptor C-CHN-BT commonly contributed to the drug-stimulated ATPase activity of ABCB1 WT and SNP variants. These data suggest that two carbocyclic systems with at least one aromatic ring (M532) as well as ring-linking groups containing one carbon atom (M132) are important structural components for the recognition by ABCB1 WT and SNP variants (Table 5). The values of coefficients corresponding to M532, M132, and C-CHN-BT are plotted for each variant in Figure 7. The values were not equal to ABCB1 WT and those SNP variants. Indeed, the A893P variant exhibited the highest values for the coefficients of M532, M132, and C-CHN-BT. Figure 8 depicts the chemical structures of verapamil, prenylamine, and nicardipine to exemplify the structural components represented by M532, M132, C-CHN-BT, and other descriptors.

In addition to M532, M132, and C-CHN-BT, other structural components also contributed the drug-stimulated ATPase activity of ABCB1 WT and SNP variants, but in unequal manners. As demonstrated in Table 5, the coefficients of CFCs and descriptors varied among WT and those variants. For example, the presence of one substituted carbon atom in an unfused aromatic ring (CFC = G010) negatively contributed the drug-stimulated ATPase activity of the I849M variants, whereas this structural component did not affect the other variants or WT. On the other hand, the benzene structure linked to the other ring by a single or double bond (CFC = M113) negatively contributed to the drug-stimulated ATPase activity of M986V, G1063A, A999T, S400N, and A893S variants and WT, whereas the activity of the other variants was not affected by this structural component. Thus, the variation of coefficients for the CFCs and descriptors listed in Table 5 appears to reflect changes in the substrate specificity owing to alterations of amino acids of ABCB1.

To facilitate our understanding in greater detail, we classified all of the tested compounds according to the CFCs and descriptors (see Table 6). For example, structural components represented by M532 are involved in verapamil, bepridil, and nicardipine, whereas those represented by M132 are in fendiline, prenylamine, and quinidine. Structural components corresponding to the descriptor of C-CHN-BT are widely found in different compounds. By referring to the descriptor coefficients (Table 5) and the corresponding descriptors involved in test compounds (Table 6), we could elucidate differences in the substrate specificity among ABCB1 WT and SNP variants.

MD Simulation. The three-dimensional structure of ABCB1 was generated by homology modeling based on the Sav1866 structure template (*37*). In the resulting homology model of ABCB1, amino acid 893 is located in the intracellular loop region connecting two transmembrane domains, i.e., TM10 and TM11 (Figure 9A). It was assumed that amino acid alterations at this position may change the loop structure and thereby affect the drug-stimulated ATPase activity (see Figures 3 and 4). To examine our hypothesis, we constructed a truncated model that consists of the intracellular loop connected with TM10 and TM11. The initial three-dimensional structure of each truncated model (A893S, A893T, or A893P) was deduced from the homology model of ABCB1. Figure 9B demonstrates the loop structures of WT, A893S, A893T, or A893P calculated from the trajectory data of MD simulations at 310 K (37 °C) for 3 ns. Our molecular dynamic simulation clearly shows that multiple kinks are formed in the intracellular loop between TM10 and TM11 in the A893P protein. The RMSF value of the α carbon of each amino acid residue was calculated from the trajectory data for the intracellular loop of WT, A893S, A893T, and A893P. The A893P variant exhibited notably great fluctuations in the intracellular loop, in particular, at the region of amino acids 910−920 (data not shown).

DISCUSSION

SNPs and Haplotypes in ABCB1. The first investigation into the effects of genetic polymorphisms of ABCB1 on pharmacotherapy was reported in 2000 (*6*). One silent SNP 3435C > T in exon 26 of the *ABCB1* gene was reportedly correlated with ABCB1 expression levels. Since that report was published, a large number of genetic variations of the human *ABCB1* gene have been discovered (*24*, *25*). Table 7 summarizes the allele frequencies of the genetic variants that were investigated in this study.

Recent findings suggest that genetic variation of 3435C > T may not be the single causal modulator of the observed functional differences (*25*). In fact, Horinouchi et al. and Kroetz et al. have provided evidence that the ABCB1 3435 site is in tight linkage disequilibrium with a number of other variant sites, including the 2677G > T variant leading to the Ala893Ser change (A893S) (*8*, *16*). Similar linkage disequilibrium was observed in West Black African populations (*23*). It is likely that genetic variations at position 2677 that result in alterations of amino acid 893 are more directly contributed to interindividual variability in ABCB1 function.

Table 5: ABCB1 WT and Variant-Specific Descriptors and Corresponding Coefficients Deduced from QSAR Analysis[a]

	coefficients (95% reliability) for ABCB1 WT and vatiants											
descriptor	WT	S400N	R492C	R669C	I849M	A893P	A893S	A893T	M986V	A999T	P1051A	G1063A
M532	24.3 (3.76)	21.2 (5.81)	18.5 (5.87)	35.9 (7.68)	52.7 (11.30)	169.8 (18.84)	14.0 (4.03)	61.2 (7.75)	39.4 (8.76)	63.0 (9.39)	13.9 (4.78)	52.1 (10.94)
M132	21.5 (3.89)	14.1 (5.34)	13.6 (5.78)	32.8 (6.89)	61.4 (12.66)	135.6 (22.95)	11.2 (4.06)	52.8 (7.16)	38.2 (8.62)	65.9 (8.44)	7.6 (5.71)	24.3 (10.46)
C-CHN-BT	3.3 (0.72)	3.8 (0.95)	1.7 (0.87)	3.5 (1.08)	5.7 (1.55)	11.6 (2.48)	1.2 (0.65)	6.1 (1.29)	7.1 (1.43)	7.3 (1.44)	2.0 (0.66)	2.8 (1.86)
ESTR				−10.1 (4.93)				−12.5 (5.00)				
OH-Ar									−6.4 (4.03)			
R-CC						16.1 (7.86)					−4.4 (1.73)	
RT		−8.9 (4.21)										−17.7 (8.22)
-O-Ar										5.7 (3.67)		
D012							5.5 (4.10)					
G010					−15.4 (9.59)							
H100			4.9 (3.59)									
H181										−7.3 (5.04)		
H421								14.6 (6.84)				
H521									14.1 (10.42)			
M113	−5.8 (3.69)	−11.7 (5.30)					−7.7 (3.70)		−22.8 (8.75)	−16.4 (8.19)		−16.5 (10.58)
M232												−14.5 (9.38)
M280	4.8 (2.65)											
M313							−5.2 (3.18)					
M332		−5.0 (3.11)										
M370			4.2 (3.14)									
M372				10.0 (5.46)	14.4 (7.91)							
M392						73.3 (25.03)					10.3 (6.38)	
M531			−5.1 (3.05)									
M540						15.8 (11.27)						
H7	7.3 (4.01)				24.0 (10.91)							
H8								10.7 (4.74)				
L1											−6.7 (2.52)	
L9				13.8 (6.93)								
constant	−12.2	−5.5	−0.2	−2.3	−24.0	−7.1	1.3	−4.3	0.9	9.0	0.6	−11.2
R^2	0.934	0.847	0.853	0.906	0.893	0.981	0.782	0.954	0.915	0.956	0.836	0.831
FO(6, 29)	68.9	26.8	28.1	46.4	40.5	254.5	17.3	100.3	51.8	106.2	24.6	23.7
Q^2	0.883	0.710	0.767	0.729	0.826	0.968	0.572	0.923	0.828	0.909	0.617	0.760

[a] R^2, correlation coefficient; FO, Fisher value (level of statistical significance).

Amino Acid 893 Is a "Hot Spot" in the Ethnic-Specific Polymorphisms of ABCB1. The present study addresses the impact of nonsynonymous polymorphisms of ABCB1 (i.e., S400N, R492C, R669C, I849M, A893S, A893T, A893P, M986V, A999T, P1051A, and G1063A) on its function. To evaluate functional changes associated with nonsynonymous polymorphisms in the present study, we measured the ATPase activity of ABCB1 variants by using structurally unrelated test compounds as potential substrates. The measurement of drug-stimulated ATPase activity was widely used by different research groups to investigate the function of ABCB1 (*1*, *33*). We here demonstrate that amino acid 893 is a hot spot in the genetic polymorphisms of ABCB1 in terms of both pharmacological and anthropological aspects.

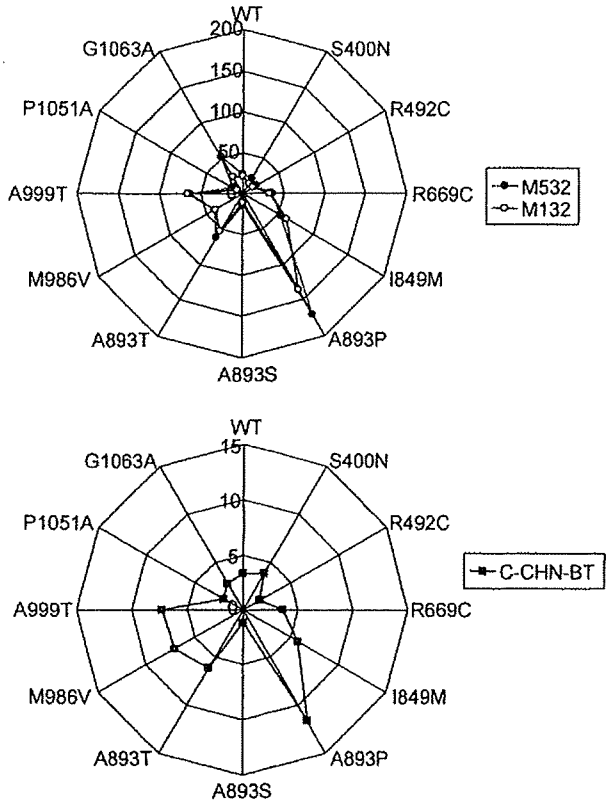

FIGURE 7: Comparison of coefficients for M532 and M132 (upper panel) as well as for C-CHN-BT (lower panel) among ABCB1 WT and SNP variants. The values of those coefficients for WT and SNP variants (i.e., S400N, R492C, R669C, I849M, A893P, A893S, A893T, M986V, A999T, P1051A, and G1063A) are the same as those shown in Table 5.

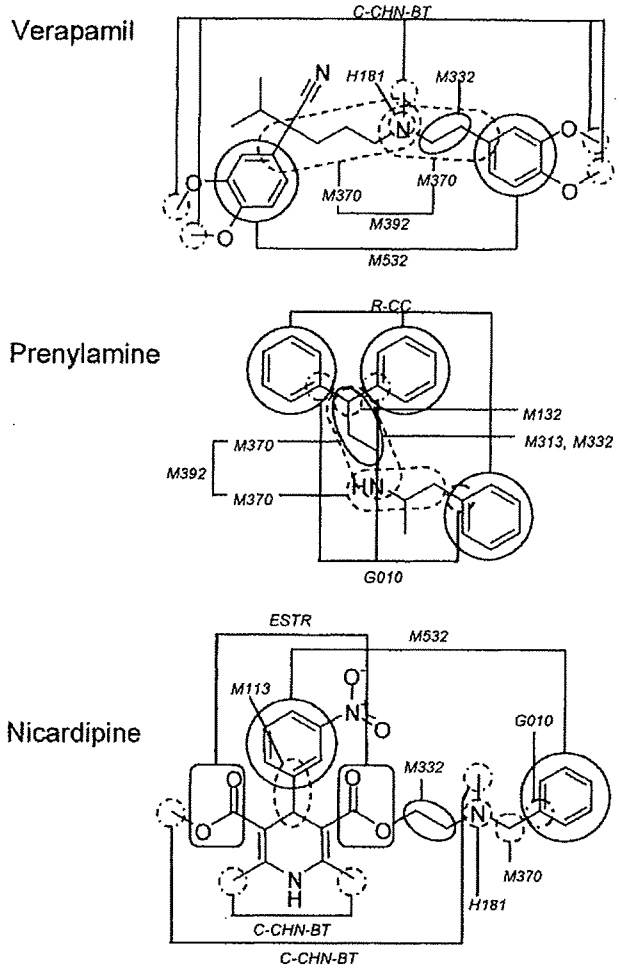

FIGURE 8: Chemical structures of verapamil, prenylamine, and nicardipine and their structural components represented by M532, M132, C-CHN-BT, and other descriptors.

As Horinouchi et al., Kroetz et al., and Allabi et al. reported, the ABCB1 G2677T/A contains a triallelic polymorphism (with G at nucleotide 2677 found in exon 21 of the WT sequence and with A and T at that position comprising the three possible variants), which results in an amino acid change Ala893Ser/Thr (A893S/T) (*8*, *16*, *23*). The polymorphisms of 2677G, 2677T, and 2677A exhibit wide ethnic differences in the allele frequency. It is important to note that the frequency of allele 2677G (Ala893) was the highest in the African population, and it decreases along the order of African-American, Mexican-American, Caucasian, Japanese, Asian-American, and Pacific Islander (Figure 10), suggesting a west−east downward geographical gradient. On the other hand, the frequency of allele 2677A shows a west−east upward geographical gradient (Figure 10). Interestingly, similar west−east upward geographical gradients are observed in the frequencies of the 421A allele of ABCG2 (*47*) and the 538A allele of ABCC11 (*48*). In the case of the genetic polymorphisms of ABCC11, we recently reported that the SNP of 538G > A is responsible for determination of earwax type (*48*). Individuals with dry earwax are AA homozygotes and are frequently observed in Northern China, Japan, and Southern Asia.

In addition to the triallelic polymorphism of 2677G > T/A, the recent NCBI SNP database contains the 2677G > C polymorphism (dbSNP: rs2032582) that results in the A893P variant. This polymorphism has not yet been well validated, and it is regarded as a rare mutation. As shown in Figures 3 and 4 as well as in Tables 2 and 3, the A893P variant exhibited remarkably high ATPase activity toward verapamil and nicardipine in the present study. There is a possibility that increased ATPase activity of this variant protein could be due to a computational method used for normalization of protein levels. However, this explanation may be oversimplified. In fact, the V_{max}/K_m value of the A893P for nicardipine was 2 orders of magnitude (118-fold) greater than that of the WT (Figure 4 and Table 2), whereas the V_{max}/K_m value for vinblastine was only 3-fold greater than that of the WT (Figure 4). These results suggest that the functional impact of the A893P substitution varies depending on the drugs tested. High ATPase activity of this variant was observed toward structurally diverse test compounds as well (Figure 5). It is interesting, but puzzling, that the 2677C allele occurs at an extremely low incidence as compared with the 2677A and 2677T alleles. ABCB1 is located in the apical domain of the enterocytes of the gastrointestinal tract (jejunum and duodenum) and limits the uptake and absorption of xenobiotics from the intestine into the systemic circulation by excreting substrates into the gastrointestinal tract. Therefore, one could assume that, because of the extremely high transport activity of this A893P variant, the uptake of nutrients can also be limited in individuals carrying the 2677C allele. If this assumption were true, it would be likely that those ancient individuals were subjected to stringent natural selection such that the allele frequency might have

Table 6: Classification of Test Compounds According to Descriptors and CFCs

descriptor	CFC	compounds									
M532	M532	verapamil	bepridil	nicardipine							
M132	M132	fendiline	prenylamine	quinidine							
C-CHN-BT	M281	epinephrine	melatonin	verapamil	diltiazem	bepridil	nicardipine	pinacidil	indomethacin	acemetacin	acetylsalicyclic acid
		ibuprofen	naproxen	vinblastine	etoposide	daunorubicin	methotrexate	doxorubicin	quinidine	novobiocin	
	M282	nifedipine	diltiazem	nicardipine	mepirizol	vinblastine	etoposide	paclitaxel	penicillin G	novobiocin	
	M283	verapamil	diltiazem	vinblastine	paclitaxel	tacrolimus					
ESTR	J211	vinblastine									
	J212	nifedipine	nicardipine								
OH-Ar	H441	serotonin	etoposide	novobiocin							
	H442	dopamine	norepinephrine	epinephrine	daunorubicin	doxorubicin					
R-CC	M531	dopamine	norepinephrine	epinephrine	nifedipine	diltiazem	pinacidil	indomethacin	acemetacin	ibuprofen	acetylsalicyclic acid
		naproxen	etoposide	daunorubicin	methotrexate	doxorubicin	PAH	penicillin G	novobiocin		
	M532	verapamil	bepridil	nicardipine							
	M533	fendiline	prenylamine	paclitaxel							
RT	H211	diltiazem	indomethacin	acemetacin	mepirizol						
-O-Ar	H541	melatonin	diltiazem	indomethacin	acemetacin	naproxen	vinblastine	daumorubicin	doxorubicin	quinidine	
D012	D012	vinblastine	etoposide	methotrexate							
G010	G010	bepridil	fendiline	prenylamine	nicardipine	paclitaxel	penicillin G				
H100	H100	glycine	glutamic acid	dopamine	norepinephrine	GABA	histamine	serotonin	daunorubicin	doxorubicin	PAH
H181	H181	glycine	glutamic acid	dopamine	norepinephrine	epinephrine	GABA	histamine	serotonin	verapamil	diltiazem
		bepridil	fendiline	prenylamine	nicardipine	vinblastine					
H421	H421	vinblastine	daunorubicin	doxorubicin	novobiocin						
H521	H521	etoposide	daunorubicin	doxorubicin							
M113	M113	nifedipine	diltiazem	nicardipine							
M232	M232	bepridil	pinacidil	ibuprofen	novobiocin						
M280	M280	glycine	glutamic acid	dopamine	norepinephrine	GABA	histamine	serotonin	fendiline	prenylamine	nicorandil
		5-fluorouracil	PAH								
M313	M313	glutamic acid	bepridil	fendiline	prenylamine	methotrexate	tacrolimus				
M332	M332	glutamic acid	dopamine	norepinephrine	epinephrine	GABA	histamine	serotonin	melatonin	verapamil	diltiazem
		bepridil	fendiline	prenylamine	nicardipine	nicorandil	paclitaxel	methotrexate			
M370	M370	dopamine	norepinephrine	epinephrine	histamine	serotonin	melatonin	verapamil	bepridil	fendiline	prenylamine
		nicardipine	indomethacin	acemetacin	ibuprofen	naproxen	paclitaxel	methotrexate	quinidine	penicillin G	
M372	M372	indomethacin	acemetacin	ibuprofen	naproxen	penicillin G					
M392	M392	verapamil	fendiline	prenylamine							
M531	M531	(refer to above)									
M540	M540	histamine	serotonin	melatonin	nicorandil	naproxen	mepirizol	vinblastine	daunorubicin	doxorubicin	5-fluorouracil
H7	H7	quinidine	glycine	glutamic acid	dopamine	norepinephrine	epinephrine	GABA	histamine	serotonin	melatonin
		verapamil	nifedipine	diltiazem	bepridil	fendiline	prenylamine	nicardipine	nicorandil	pinacidil	acetylsalicylic acid
		indomethacin	acemetacin	ibuprofen	naproxen	mepirizol	vinblastine	etoposide	daunorubicin	paclitaxel	methotrexate
		doxorubicin	5-fluorouracil	PAH	penicillin G						
H8	H8	glycine	glutamic acid	GABA	histamine	nifedipine	fendiline	prenylamine	nicardipine	nicorandil	acetylsalicylic acid
		pinacidil	ibuprofen	methotrexate	5-fluorouracil	PAH	penicillin G				
L1	L1	nifedipine	diltiazem	nicardipine	nicorandil	mepirizol	daunorubicin	methotrexate	doxorubicin	5-fluorouracil	penicillin G
		tacrolimus	novobiocin								
L9	L9	verapamil	nifedipine	nicardipine	nicorandil	pinacidil					

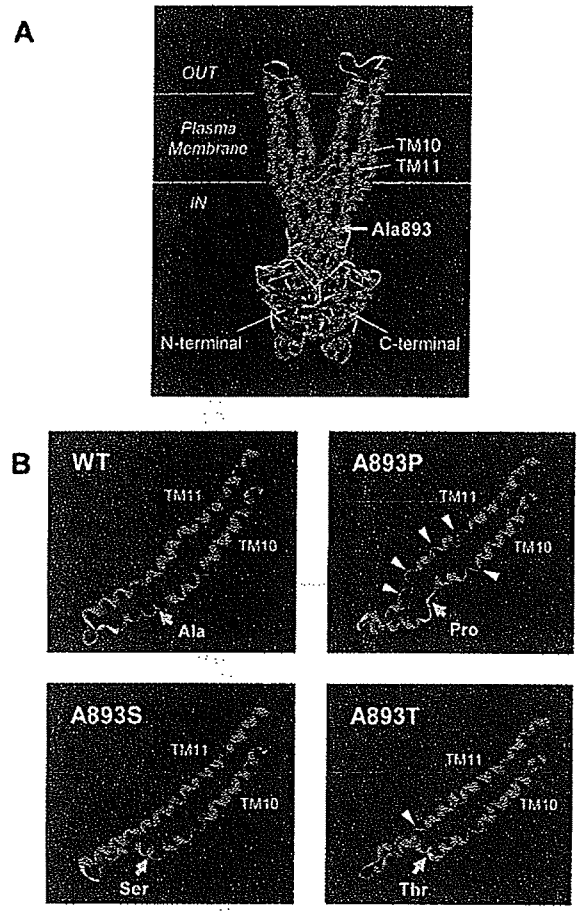

FIGURE 9: (A) Homology model structure of human ABCB1. Homology modeling was performed by using the Sav1866 structure (*37*) as a template. (B) Structure of the intracellular loop between TM10 and TM11 calculated by MD simulation. Detailed conditions used for homology modeling and MD simulation are described in Experimental Procedures.

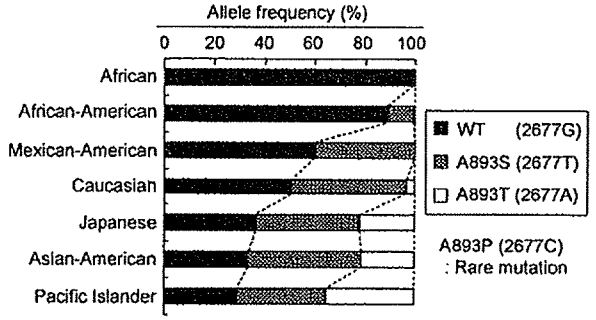

FIGURE 10: Allele frequencies of WT (Ala893), A893S (Ser893), and A893T (Thr893) among different ethnic populations. Those allele frequencies were calculated from the currently available data (*8*, *16*, *23*, *29*–*31*) and are represented as bars in this graph. The A893P (Pro893) variant is a rare mutation (rs2032582) recorded in the NCBI dbSNP database.

been maintained at minimal levels throughout the history of *Homo sapiens*.

In contrast to the A893P variant, the A893S variant exhibited the lowest V_{max}/K_m values toward verapamil or nicardipine among the variants tested (Tables 2 and 3). The 2677T polymorphism causing this A893S variant has recently been reported to be crucial in conferring susceptibility to lung cancer (*49*). It is suggested that the 2677T mutation results in a decreased transport of environmental carcinogens out of pulmonary cells. The A893T variant, on the other hand, exhibited V_{max}/K_m values even higher than those of WT (Tables 2 and 3). Amino acid 893 is located in the intracellular loop between TM10 and TM11 (Figure 1), and amino acid alterations at this position appear to affect the function of ABCB1.

MD Simulation of the Intracellular Loop between TM10 and TM11. Most recently, Dawson and Locher demonstrated the three-dimensional structure of Sav1866, a bacterial ABC transporter (*37*). As with ABCB1, the ATPase activity of Sav1866 was stimulated by doxorubicin and vinblastine (*37*). Sav1866 is a half ABC transporter, showing significant similarity to human ABCB1. In the present study, the putative three-dimensional structure of ABCB1 WT (Figure 9A) was deduced from X-ray crystallography of Sav1866 by means of homology modeling. To understand the molecular mechanisms underlying the observed differences in the ATPase activity among ABCB1 WT, A893P, A893S, and A893T (Figures 3–5), we performed MD simulation based on the homology model of ABCB1.

According to multiple alignments, A893 residing in the second half of human ABCB1 corresponds to V199 of Sav1866. It is important to note that V199 in the Sav1866 structure is located in the cytoplasmic helical stretch in continuity with TM4 before "coupling helix 2". Dawson and Locher emphasize the importance of the intracellular loop regions, in particular, of "coupling helices 1 and 2". In the case of ABCB1, coupling helix 2 corresponds to amino acid residues 903–912. Our MD simulation data (Figure 9B) suggest that the A893P mutation promotes multiple kinks in this cytoplasmic helical region and modifies the interaction of coupling helix 2 with the ATP-binding domain. This may provide an explanation, in part, for the effect of the A893P mutation on ATP hydrolysis. Loo et al. have recently suggested that rearrangement of TM11 may contribute to the release of drug substrate during ATP hydrolysis (*50*). More detailed MD simulation of ABCB1 is presently ongoing in our laboratory, and results will be reported elsewhere.

Functional Evaluation of Genetic Polymorphisms of ABCB1 by QSAR Analysis. Other nonsynonymous polymorphisms, such as S400N, R492C, R669C, P1051A, and G1063A occurring in intracellular loops as well as I849M, M986V, and A999T alterations in transmembrane domains, exhibited moderate changes in the kinetic properties of ABCB1. To understand the impact of those nonsynonymous polymorphisms on the function of ABCB1, it is critically important to quantitatively analyze the functional differences among such variants. To accomplish this, we have developed a method of QSAR analysis. Using the high-speed screening system, we first measure ABCB1 ATPase activity toward a total of 41 different therapeutic drugs and compounds.

On the basis of the ATPase activity data, we could analyze the QSAR to identify multiple sets of CFCs closely linked with the substrate specificity of ABCB1 WT and SNP variants. We used CFCs to describe the chemical structures of a variety of substrates and nonsubstrates for ABCB1. The CFCs were originally created to answer the need for accessing information in the increasing numbers of chemical patents. Derwent Information, Ltd., developed this structure-indexing language, which is suitable for describing chemical

Table 7: Allele Frequencies of ABCB1 SNPs Investigated in This Study[a]

position and change					wild type		variant type		
amino acid	cDNA		ethnic group	no. of samples	allele	frequency (%)	allele	frequency (%)	ref
S400N	1199	G > A	African	111	G	100.0	A	0.0	*23*
			African-American	100	G	99.0	A	1.0	*16*
			German	461	G	94.5	A	5.5	*29*
			Caucasian	85	G	87.1	A	12.9	*6*
			Caucasian	50	G	98.0	A	2.0	*31*
			Caucasian	100	G	97.5	A	2.5	*16*
			Mexican-American	10	G	100.0	A	0.0	*16*
			Asian-American	30	G	100.0	A	0.0	*16*
			Pacific Islander	7	G	100.0	A	0.0	*16*
R492C	1474	C > T	African-American	23	C	100.0	T	0.0	*7*
			Caucasian	37	C	98.6	T	1.4	*7*
R669C	2005	C > T	African-American	100	C	99.0	T	1.0	*16*
			Caucasian	100	C	100.0	T	0.0	*16*
			Mexican-American	10	C	100.0	T	0.0	*16*
			Asian-American	30	C	100.0	T	0.0	*16*
			Pacific Islander	7	C	100.0	T	0.0	*16*
I849M	2547	A > G	African-American	100	C	100.0	T	0.0	*16*
			Caucasian	100	C	99.5	T	0.5	*16*
			Mexican-American	10	C	100.0	T	0.0	*16*
			Asian-American	30	C	100.0	T	0.0	*16*
			Pacific Islander	7	C	100.0	T	0.0	*16*
A893P/S/T	2677	G > T/A/C	African (Beninese)	111	G	99.1	T	0.9	*23*
							A	0.0	
			African-American	100	G	89.5	T	10.0	*16*
							A	0.5	
			Caucasian	100	G	50.0	T	46.5	*16*
							A	3.5	
			Caucasian	50	G	52.0	T	38.0	*31*
							A	10.0	
			German	461	G	56.5	T	41.6	*29*
							A	1.9	
			Mexican-American	10	G	60.0	T	40.0	*16*
							A	0.0	
			Asian-American	30	G	33.3	T	45.0	*16*
							A	21.7	
			Japanese	117	G	44.0	T	35.5	*8*
							A	20.5	
			Japanese (placenta)	100	G	43.0	T	39.0	*30*
							A	18.0	
			Japanese	48	G	36.5	T	41.7	*30*
							A	21.8	
			Pacific Islander	7	G	28.6	T	35.7	*16*
							A	35.7	
			ND	ND	G	ND	C	ND	NCBI dbSNP (rs2032582)
M986V	2956	A > G	Japanese (placenta)	100	A	99.5	G	0.5	*30*
			Japanese	48	A	100.0	G	0.0	*30*
A999T	2995	G > A	cell lines	36	G	94.4	A	5.6	*28*
P1051A	3151	C > G	African-American	100	C	99.5	G	0.5	*16*
			Caucasian	100	C	100.0	G	0.0	*16*
			Mexican-American	10	C	100.0	G	0.0	*16*
			Asian-American	30	C	100.0	G	0.0	*16*
			Pacific Islander	7	C	100.0	G	0.0	*16*
G1063A	3188	G > A	ND	ND	G	ND	A	ND	NCBI dbSNP (rs2707944)

[a] ND, not determined.

structures. Markush TOPFRAG is the software that generates the CFCs from chemical structure information.

The uniqueness of this approach derives from the fact that ABCB1 ATPase activity is described as a linear combination of CFCs and that the coefficient for each CFC reflects the extent of the contribution of a specific chemical moiety to the ATPase activity. As demonstrated in Table 5 and Figure 7, there is a large variation among the SNP variants in terms of the CFCs contributing to the ATPase activity, suggesting that nonsynonymous polymorphisms influence the substrate specificity of ABCB1 (Table. 6). The point in the catalytic cycle at which substrate binding takes place and details of how ATP hydrolysis drives transport may be critical for understanding the mechanism of substrate specificity (*51*).

Concluding Remarks The effect of SNPs on the transport activity appears to depend on the substrates tested, and therefore the functional analysis of SNPs by using a wide variety of substrates is of great interest. This concept was verified by our recent study on the genetic polymorphisms of human ABCG2 (*52*, *53*). One amino acid substitution can alter interactions between the active site of an ABC transporter and substrate molecules. Therefore, it is critically

important to quantitatively analyze and evaluate such structure-related interactions. In this context, the new QSAR analysis with CFCs will provide a powerful tool to quantify the impact of genetic polymorphisms on the function of ABC transporters. If the chemical structure of a test compound is available, we are able to predict the effect of SNPs on the substrate specificity of ABCB1 toward the compound by using our QSAR analysis method. The validity of our QSAR analysis method was proven in our recent studies where troglitazone and gefitinib were predicted to be strong inhibitors for ABCB11 (*54*) and ABCG2 (*55*), respectively. It is also possible to further expand this QSAR analysis with a larger number of structurally unrelated compounds, if needed.

ACKNOWLEDGMENT

The first and second authors equally contributed to this study. The authors thank Drs. Deanna L. Kroetz and Kathleen M. Giacomini (Department of Biopharmaceutical Sciences, University of California San Francisco, San Francisco, CA) for their kind advice on the haplotype in the human *ABCB1* gene.

REFERENCES

1. Ambudkar, S. V., Lelong, I. H., Zhang, J., and Cardarelli, C. (1998) Purification and reconstitution of human P-glycoprotein, *Methods Enzymol. 292*, 492−504.
2. Gottesman, M. M., and Ling, V. (2006) The molecular basis of multidrug resistance in cancer: the early years of P-glycoprotein research, *FEBS Lett. 580*, 998−1009.
3. Schinkel, A. H., Smit, J. J., van Tellingen, O., Beijnen, J. H., Wagenaar, E., van Deemter, L., Mol, C. A., van der Valk, M. A., Robanus-Maandag, E. C., te Riele, H. P. J., Bernsd, A. J. M., and Borst, P. (1994) Disruption of the mouse mdr1a P-glycoprotein gene leads to a deficiency in the blood-brain barrier and to increased sensitivity to drugs, *Cell 77*, 491−502.
4. Virgintino, D., Robertson, D., Errede, M., Benagiano, V., Tauer, U., Roncali, L., and Bertossi, M. (2002) Expression of caveolin-1 in human brain microvessels, *Neuroscience 115*, 145−152.
5. Kerb, R., Hoffmeyer, S., and Brinkmann, U. (2001) ABC drug transporters: hereditary polymorphisms and pharmacological impact in MDR1, MRP1 and MRP2, *Pharmacogenomics 2*, 51−64.
6. Hoffmeyer, S., Burk, O., von Richter, O., Arnold, H. P., Brockmoller, J., Johne, A., Cascorbi, I., Gerloff, T., Roots, I., Eichelbaum, M., and Brinkmann, U. (2000) Functional polymorphisms of the human multidrug-resistance gene: multiple sequence variations and correlation of one allele with P-glycoprotein expression and activity in vivo, *Proc. Natl. Acad. Sci. U.S.A. 97*, 3473−3478.
7. Kim, R. B., Leake, B. F., Choo, E. F., Dresser, G. K., Kubba, S. V., Schwarz, U. I., Taylor, A., Xie, H. G., McKinsey, J., Zhou, S., Lan, L. B., Schuetz, J. D., Schuetz, E. G., and Wilkinson, G. R. (2001) Identification of functionally variant MDR1 alleles among European Americans and African Americans, *Clin. Pharmacol. Ther. 70*, 189−199.
8. Horinouchi, M., Sakaeda, T., Nakamura, T., Morita, Y., Tamura, T., Aoyama, N., Kasuga, M., and Okumura, K. (2002) Significant genetic linkage of MDR1 polymorphisms at positions 3435 and 2677: functional relevance to pharmacokinetics of digoxin, *Pharm. Res. 19*, 1581−1585.
9. Itoda, M., Saito, Y., Komamura, K., Ueno, K., Kamakura, S., Ozawa, S., and Sawada, J. (2002) Twelve novel single nucleotide polymorphisms in ABCB1/MDR1 among Japanese patients with ventricular tachycardia who were administered amiodarone, *Drug Metab. Pharmacokinet. 17*, 566−571.
10. Johne, A., Kopke, K., Gerloff, T., Mai, I., Rietbrock, S., Meisel, C., Hoffmeyer, S., Kerb, R., Fromm, M. F., Brinkmann, U., Eichelbaum, M., Brockmoller, J., Cascorbi, I., and Roots, I. (2002) Modulation of steady-state kinetics of digoxin by haplotypes of the P-glycoprotein MDR1 gene, *Clin. Pharmacol. Ther. 72*, 584−594.
11. Macphee, I. A., Fredericks, S., Tai, T., Syrris, P., Carter, N. D., Johnston, A., Goldberg, L., and Holt, D. W. (2002) Tacrolimus pharmacogenetics: polymorphisms associated with expression of cytochrome p4503A5 and P-glycoprotein correlate with dose requirement, *Transplantation 74*, 1486−1489.
12. Saito, S., Iida, A., Sekine, A., Miura, Y., Ogawa, C., Kawauchi, S., Higuchi, S., and Nakamura, Y. (2002) Three hundred twenty-six genetic variations in genes encoding nine members of ATP-binding cassette, subfamily B (ABCB/MDR/TAP), in the Japanese population, *J. Hum. Genet. 47*, 38−50.
13. Siegmund, W., Ludwig, K., Giessmann, T., Dazert, P., Schroeder, E., Sperker, B., Warzok, R., Kroemer, H. K., and Cascorbi, I. (2002) The effects of the human MDR1 genotype on the expression of duodenal P-glycoprotein and disposition of the probe drug talinolol, *Clin. Pharmacol. Ther. 72*, 572−583.
14. Evans, W. E., and McLeod, H. L. (2003) Pharmacogenomics−drug disposition, drug targets, and side effects, *N. Engl. J. Med. 348*, 538−549.
15. Kafka, A., Sauer, G., Jaeger, C., Grundmann, R., Kreienberg, R., Zeillinger, R., and Deissler, H. (2003) Polymorphism C3435T of the MDR-1 gene predicts response to preoperative chemotherapy in locally advanced breast cancer, *Int. J. Oncol. 22*, 1117−1121.
16. Kroetz, D. L., Pauli-Magnus, C., Hodges, L. M., Huang, C. C., Kawamoto, M., Johns, S. J., Stryke, D., Ferrin, T. E., DeYoung, J., Taylor, T., Carlson, E. J., Herskowitz, I., Giacomini, K. M., and Clark, A. G. (2003) Sequence diversity and haplotype structure in the human ABCB1 (MDR1, multidrug resistance transporter) gene, *Pharmacogenetics 13*, 481−494.
17. Saito, K., Miyake, S., Moriya, H., Yamazaki, M., Itoh, F., Imai, K., Kurosawa, N., Owada, E., and Miyamoto, A. (2003) Detection of the four sequence variations of MDR1 gene using TaqMan MGB probe based real-time PCR and haplotype analysis in healthy Japanese subjects, *Clin. Biochem. 36*, 511−518.
18. Sakaeda, T., Nakamura, T., and Okumura, K. (2003) Pharmacogenetics of MDR1 and its impact on the pharmacokinetics and pharmacodynamics of drugs, *Pharmacogenomics 4*, 397−410.
19. Weinshilboum, R. (2003) *N. Engl. J. Med.*, 529−537.
20. Marzolini, C., Paus, E., Buclin, T., and Kim, R. B. (2004) Polymorphisms in human MDR1 (P-glycoprotein): recent advances and clinical relevance, *Clin. Pharmacol. Ther. 75*, 13−33.
21. Ozawa, S., Soyama, A., Saeki, M., Fukushima-Uesaka, H., Itoda, M., Koyano, S., Sai, K., Ohno, Y., Saito, Y., and Sawada, J. (2004) Ethnic differences in genetic polymorphisms of CYP2D6, CYP2C19, CYP3As and MDR1/ABCB1, *Drug Metab. Pharmacokinet. 19*, 83−95.
22. Uwai, Y., Masuda, S., Goto, M., Motohashi, H., Saito, H., Okuda, M., Nakamura, E., Ito, N., Ogawa, O., and Inui, K. (2004) Common single nucleotide polymorphisms of the MDR1 gene have no influence on its mRNA expression level of normal kidney cortex and renal cell carcinoma in Japanese nephrectomized patients, *J. Hum. Genet. 49*, 40−45.
23. Allabi, A. C., Horsmans, Y., Issaoui, B., and Gala, J. L. (2005) Single nucleotide polymorphisms of ABCB1 (MDR1) gene and distinct haplotype profile in a West Black African population, *Eur. J. Clin. Pharmacol. 61*, 97−102.
24. Sakurai, A., Tamura, A., Onishi, Y., and Ishikawa, T. (2005) Genetic polymorphisms of ATP-binding cassette transporters ABCB1 and ABCG2: therapeutic implications, *Expert Opin. Pharmacother. 6*, 2455−2473.
25. Sakaeda, T. (2005) MDR1 genotype-related pharmacokinetics: fact or fiction?, *Drug Metab. Pharmacokinet. 20*, 391−414.
26. Green, H., Soderkvist, P., Rosenberg, P., Horvath, G., and Peterson, C. (2006) mdr-1 single nucleotide polymorphisms in ovarian cancer tissue: G2677T/A correlates with response to paclitaxel chemotherapy, *Clin. Cancer Res. 12*, 854−849.
27. Kimchi-Sarfaty, C., Oh, J. M., Kim, I. W., Sauna, Z. E., Calcagno, A. M., Ambudkar, S. V., and Gottesman, M. M. (2007) A "silent" polymorphism in the MDR1 gene changes substrate specificity, *Science 315*, 525−528.
28. Mickley, L. A., Lee, J. S., Weng, Z., Zhan, Z., Alvarez, M., Wilson, W., Bates, S. E., and Fojo, T. (1998) Genetic polymorphism in MDR-1: a tool for examining allelic expression in normal cells, unselected and drug-selected cell lines, and human tumors, *Blood 91*, 1749−1756.
29. Cascorbi, I., Gerloff, T., Johne, A., Meisel, C., Hoffmeyer, S., Schwab, M., Schaeffeler, E., Eichelbaum, M., Brinkmann, U., and Roots, I. (2001) Frequency of single nucleotide polymorphisms

in the P-glycoprotein drug transporter MDR1 gene in white subjects, *Clin. Pharmacol. Ther. 69*, 169−174.
30. Tanabe, M., Ieiri, I., Nagata, N., Inoue, K., Ito, S., Kanamori, Y., Takahashi, M., Kurata, Y., Kigawa, J., Higuchi, S., Terakawa, N., and Otsubo, K. (2001) Expression of P-glycoprotein in human placenta: relation to genetic polymorphism of the multidrug resistance (MDR)-1 gene, *J. Pharmacol. Exp. Ther. 297*, 1137−1143.
31. Gerloff, T., Schaefer, M., Johne, A., Oselin, K., Meisel, C., Cascorbi, I., and Roots, I. (2002) MDR1 genotypes do not influence the absorption of a single oral dose of 1 mg digoxin in healthy white males, *Br. J. Clin. Pharmacol. 54*, 610−616.
32. Ishikawa, T., Sakurai, A., Kanamori, Y., Nagakura, M., Hirano, H., Takarada, Y., Yamada, K., Fukushima, K., and Kitajima, M. (2005) High-speed screening of human ATP-binding cassette transporter function and genetic polymorphisms: new strategies in pharmacogenomics, *Methods Enzymol. 400*, 485−510.
33. Sarkadi, B., Price, E. M., Boucher, R. C., Germann, U. A., and Scarborough, G. A. (1992) Expression of the human multidrug resistance cDNA in insect cells generates a high activity drug-stimulated membrane ATPase, *J. Biol. Chem. 267*, 4854−4858.
34. Onishi, Y., Hirano, H., Nakata, K., Oosumi, K., Nagakura, M., Tarui, S., and Ishikawa, T. (2003) High-speed screening and structure-activity relationship analysis for the substrate specificity of P-glycoprotein (ABCB1), *Chem-Bio Inf. J. 3*, 175−193.
35. Thompson, J. D., Gibson, T. J., Plewniak, F., Jeanmougin, F., and Higgins, D. G. (1997) The CLUSTAL_X windows interface: flexible strategies for multiple sequence alignment aided by quality analysis tools, *Nucleic Acids Res. 25*, 4876−4882.
36. Sali, A., and Blundell, T. L. (1993) Comparative protein modelling by satisfaction of spatial restraints, *J. Mol. Biol. 234*, 779−815.
37. Dawson, R. J., and Locher, K. P. (2006) Structure of a bacterial multidrug ABC transporter, *Nature 443*, 180−185.
38. Hrycyna, C. A., Airan, L. E., Germann, U. A., Ambudkar, S. V., Pastan, I., and Gottesman, M. M. (1998) Structural flexibility of the linker region of human P-glycoprotein permits ATP hydrolysis and drug transport, *Biochemistry 37*, 13660−13673.
39. Fiser, A., Do, R. K., and Sali, A. (2000) Modeling of loops in protein structures, *Protein Sci. 9*, 1753−1773.
40. Vriend, G. (1990) WHAT IF: a molecular modeling and drug design program, *J. Mol. Graphics 8*, 52−56.
41. Laskowski, R. A., MacArthur, M. W., Moss, D. S., and Thornton, J. M. (1993) PROCHECK: a program to check the stereochemical quality of protein structures, *J. Appl. Crystallogr. 26*, 283−291.
42. Case, D. A., Darden, T. A., Cheatham, T. E., III, Simmerling, C. L., Wang, J., Duke, R. E., Luo, R., Merz, K. M., Wang, B., Pearlman, D. A., Crowley, M., Brozell, S., Tsui, V., Gohlke, H., Mongan, J., Hornak, V., Cui, G., Beroza, P., Schafmeister, C., Caldwell, J. W., Ross, W. S., and Kollman, P. A. (2004) University of California, San Francisco.
43. Onufriev, A., Bashford, D., and Case, D. A. (2000) Modification of the generalized Born model suitable for macromolecules, *J. Phys. Chem. B 104*, 3712−3720.
44. Berendsen, H. J. C., Postma, J. P. M., van Gunsteren, W. F., DiNola, A., and Haak, J. R. (1984) Molecular dynamics with coupling to an external bath, *J. Chem. Phys. 81*, 3684−3690.
45. Ryckaert, J., Ciccotti, G., and Berendsen, H. J. C. (1977) Numerical integration of the cartesian equations of motion of a system with constraints: molecular dynamics of *n*-alkanes, *J. Comput. Phys. 23*, 327−341.
46. Georges, E., Bradley, G., Gariepy, J., and Ling, V. (1990) Detection of P-glycoprotein isoforms by gene-specific monoclonal antibodies, *Proc. Natl. Acad. Sci. U.S.A. 87*, 152−156.
47. Ishikawa, T., Tamura, A., Saito, H., Wakabayashi, K., and Nakagawa, H. (2005) Pharmacogenomics of the human ABC transporter ABCG2: from functional evaluation to drug molecular design, *Naturwissenschaften 92*, 451−463.
48. Yoshiura, K., Kinoshita, A., Ishida, T., Ninokata, A., Ishikawa, T., Kaname, T., Bannai, M., Tokunaga, K., Sonoda, S., Komaki, R., Ihara, M., Saenko, V. A., Alipov, G. K., Sekine, I., Komatsu, K., Takahashi, H., Nakashima, M., Sosonkina, N., Mapendano, C. K., Ghadami, M., Nomura, M., Liang, D. S., Miwa, N., Kim, D. K., Garidkhuu, A., Natsume, N., Ohta, T., Tomita, H., Kaneko, A., Kikuchi, M., Russomando, G., Hirayama, K., Ishibashi, M., Takahashi, A., Saitou, N., Murray, J. C., Saito, S., Nakamura, Y., and Niikawa, N. (2006) A SNP in the ABCC11 gene is the determinant of human earwax type, *Nat. Genet. 38*, 324−330.
49. Gervasini, G., Carrillo, J. A., Garcia, M., San Jose, C., Cabanillas, A., and Benitez, J. (2006) Adenosine triphosphate-binding cassette B1 (ABCB1) (multidrug resistance 1) G2677T/A gene polymorphism is associated with high risk of lung cancer, *Cancer 107*, 2850−2857.
50. Loo, T. W., Bartlett, M. C., and Clarke, D. M. (2005) ATP hydrolysis promotes interactions between the extracellular ends of transmembrane segments 1 and 11 of human multidrug resistance P-glycoprotein, *Biochemistry 44*, 10250−10258.
51. Ambudkar, S. V., Kim, I. W., and Sauna, Z. E. (2006) The power of the pump: Mechanisms of action of P-glycoprotein (ABCB1), *Eur. J. Pharm. Sci. 27*, 392−400.
52. Tamura, A., Watanabe, M., Saito, H., Nakagawa, H., Kamachi, T., Okura, I., and Ishikawa, T. (2006) Functional validation of the genetic polymorphisms of human ATP-binding cassette (ABC) transporter ABCG2: identification of alleles that are defective in porphyrin transport, *Mol. Pharmacol. 70*, 287−296.
53. Tamura, A., Wakabayashi, K., Onishi, Y., Takeda, M., Ikegami, Y., Sawada, S., Tsuji, M., Matsuda, Y., and Ishikawa, T. (2007) Re-evaluation and functional classification of non-synonymous single nucleotide polymorphisms of the human ATP-binding cassette transporter ABCG2, *Cancer Sci. 98*, 231−239.
54. Hirano, H., Kurata, A., Onishi, Y., Sakurai, A., Saito, H., Nakagawa, H., Nagakura, M., Tarui, S., Kanamori, Y., Kitajima, M., and Ishikawa, T. (2006) High-speed screening and QSAR analysis of human ATP-binding cassette transporter ABCB11 (bile salt export pump) to predict drug-induced intrahepatic cholestasis, *Mol. Pharmaceutics 3*, 252−265.
55. Saito, H., Hirano, H., Nakagawa, H., Fukami, T., Oosumi, K., Murakami, K., Kimura, H., Kouchi, T., Konomi, M., Tao, E., Tsujikawa, N., Tarui, S., Nagakura, M., Osumi, M., and Ishikawa, T. (2006) A new strategy of high-speed screening and quantitative structure-activity relationship analysis to evaluate human ATP-binding cassette transporter ABCG2-drug interactions, *J. Pharmacol. Exp. Ther. 317*, 1114−1124.

BI700330B

J Hum Genet (2007) 52:686–689
DOI 10.1007/s10038-007-0165-y

SHORT COMMUNICATION

A Japanese patient with a mild Lenz–Majewski syndrome

Sumito Dateki · Tatsuro Kondoh · Gen Nishimura · Katsuaki Motomura · Koh-ichiro Yoshiura · Akira Kinoshita · Hideo Kuniba · Yoshiyuki Koga · Hiroyuki Moriuchi

Received: 10 April 2007 / Accepted: 17 May 2007 / Published online: 26 June 2007

Abstract We report on a sclerosing bone dysplasia, associated with cutis laxa, enamel dysplasia, and mental retardation. The patient was a 17-year-old Japanese boy of normal height and muscular build. Cutis laxa with prominent veins in the scalp and abdominal wall and delayed eruption of permanent teeth attracted the attention of clinicians in infancy and adolescence, respectively. The clinical manifestations included a progeroid facial appearance with prognathism, wrinkled skin, and interdigital webbing. The intelligence quotient was estimated at 60. Enamel dysplasia was histologically confirmed. Skeletal changes included calvarial hyperostosis, sclerosis of the skull base, an enlarged, sclerotic mandible, broad clavicles and ribs, and diaphyseal undermodeling of the tubular bones. Metaepiphyseal sclerosis or longitudinal striation was found in the long bones. Metaphyseal equivalents of the axial skeleton showed dense osteosclerosis. These clinical and radiological manifestations overlapped with those of Lenz–Majewski syndrome. Unlike the classical phenotype of the disorder, however, he did not show brachymesophalangy with proximal symphalangism or growth failure. The present case may be considered to fall in the mildest end in the phenotypic continuum of Lenz–Majewski syndrome, suggesting that the clinical spectrum of the disorder may be broader than currently thought.

Keywords Cranial sclerosis · Cutis laxa · Lenz–Majewski syndrome · Mental retardation · Progeria

S. Dateki (✉) · T. Kondoh · K. Motomura · H. Moriuchi
Department of Pediatrics,
Nagasaki University Graduate School of Biomedical Sciences,
1-7-1, Sakamoto, Nagasaki 852-8501, Japan
e-mail: sum826@net.nagasaki-u.ac.jp

G. Nishimura
Department of Radiology, Tokyo Metropolitan Kiyose Children's Hospital, Tokyo, Japan

K. Yoshiura · A. Kinoshita · H. Kuniba
Department of Human Genetics,
Nagasaki University Graduate School of Biomedical Sciences, Nagasaki, Japan

Y. Koga
Division of Oral Pathology and Bone Metabolism,
Department of Developmental and Reconstructive Medicine,
Nagasaki University Graduate School of Biomedical Sciences,
Nagasaki, Japan

Introduction

Lenz–Majewski syndrome (LMS) (OMIM 151050) is a rare sclerosing bone dysplasia, first described by Braham (1969) in 1969 and subsequently named Lenz–Majewski hyperostotic dwarfism (Lenz and Majewski 1974; Robinow et al. 1977). Only nine affected individuals have been reported to date, and all were sporadic (Braham 1969; Macpherson 1974; Kaye et al. 1974; Lenz and Majewski 1974; Robinow et al. 1977; Gorlin and Whitley 1983; Chrzanowska et al. 1989; Nishimura et al. 1997; Saraiva 2000; Wattanasirichaigoon et al. 2004). The skeletal changes include progressive hyperostosis of the craniofacial bones with delayed closure of the fontanelles, diaphyseal cortical thickening of the tubular bones, and brachymesophalangy with proximal symphalangism. In addition, affected individuals show moderate to severe mental retardation, severe growth failure, cutis laxa, enamel hypoplasia, choanal atresia, nasolacrimal duct obstruction, and webbed fingers and toes. The prognosis is

guarded. Most patients that have been reporteddied during childhood (Braham 1969; Macpherson 1974; Kaye et al. 1974; Majewski 2000). We report here on a Japanese boy whose manifestations can be considered to be a mild variant of LMS. Our experience raises the suspicion that the phenotypic range of LMS is broader than currently believed.

Clinical report

The patient was a 17-year-old Japanese boy born to nonconsanguineous healthy parents who were respectively 25 (mother) and 30 (father) years old at his birth. The family history was unremarkable. He was vaginally delivered at 40 weeks of gestation after an uneventful pregnancy. Apgar scores at 1 and 5 min were 8 and 10, respectively. Birth weight was 2300 g (−2.25 SD), length was 45 cm (−1.9 SD), and head circumference was 32.5 cm (−0.7 SD). Cutis laxa and prominent veins in the scalp and abdominal wall attracted medical attention in infancy, but a skin biopsy was not contributory. Psychomotor development was mildly retarded, with the infant showing head control at 6 months, walking alone at 20 months, and speaking meaning words at 24 months. Deciduous teeth were reported to have erupted at 2 years of age. The lack of eruptions of some permanent teeth in the upper jaw at 13 years of age was the basis for his referral to our hospital for further evaluation. His four maxillary permanent teeth of central and lateral incisors did not erupt. He had also a follicular cyst around the anterior teeth, necessitating surgical extirpation. Enamel dysplasia was histologically confirmed. He showed a distinctive, progeroid facial appearance with sparse hair, large auricles, maxillar hypoplasia, high-arched palate, and prognathism (Fig. 1a,

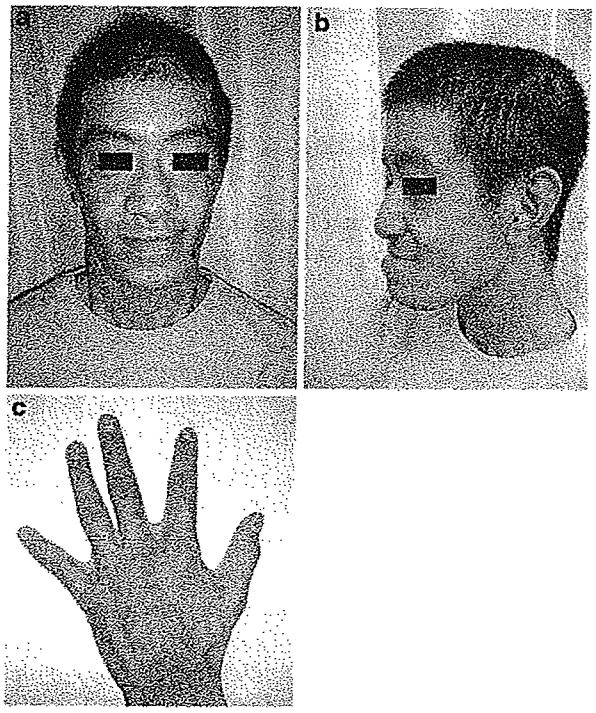

Fig. 1 Clinical photographs at 17 years of age. **a**, **b** A progeroid facial appearance with sparse hair, large auricles, and prognathism. **c** Interdigital webbing

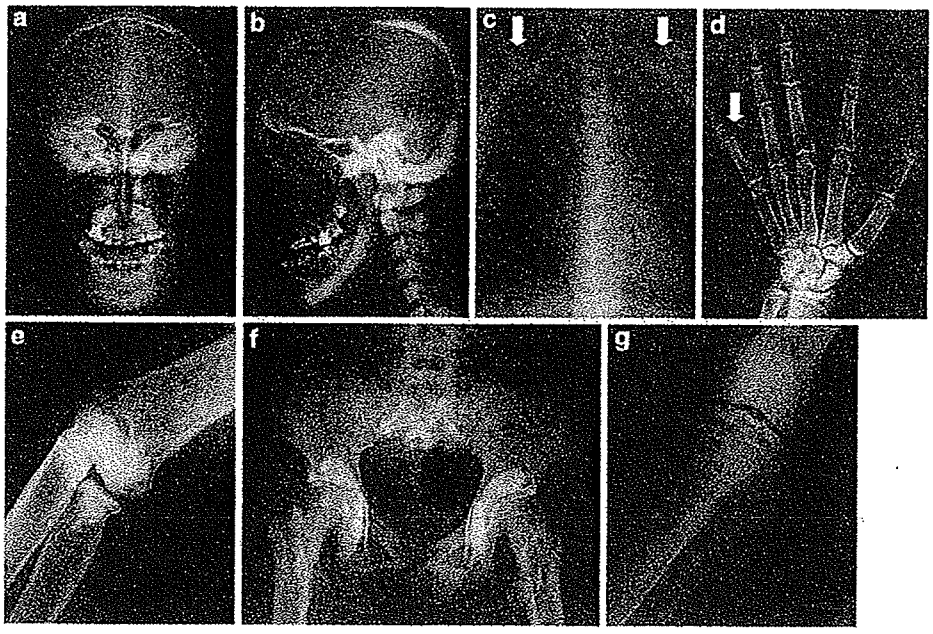

Fig. 2 Radiological findings at 17 years of age. **a**, **b** Hyperostosis of the calvaria, skull base and mandible. **c** Broad clavicles (*arrows*) and ribs, and sclerosis of metaphyseal equivalents of the spine. **d** Undermodeling of the short tubular bones and sclerosis of the carpal bones. **e** Metaepiphyseal sclerosis of the distal humerus, proximal ulna, and proximal radius. **f** Sclerosis of the sacrum, acetabulum, and proximal femur. **g** Sclerotic striations in the distal femur and proximal tibia

Table 1 Clinical and radiological findings of Lenz–Majewski syndrome (LMS)

Features	Typical LMS								Atypical LMS		Number of report ($n = 10$)
	Braham (1969); Macpherson (1974)	Lenz and Majewski (1974)	Kaye et al. (1974)	Robinow et al. (1977)	Gorlin and Whitley (1983)	Saraiva (2000)	Wattanasiri-chaigoon et al. (2004)	Chrzanowska et al.(1989)	Nishimura et al. (1997)	Our case	
Sex	Male	Female	Male	Male	Male	Female	Female	Male	Male	Male	
Gestational age	ND	Term	40 weeks	Term	Term	37 weeks	Term	Term	25 weeks	40 weeks	
Birth measurements											
Length (cm)	ND	45	ND	44.5	47	45	40	52	36	45	
Weight (g)	ND	2650	2300	2395	2800	3470	2100	2550	886	2300	
Head circumference (cm)	ND	34	ND	31.1	35	33	30	35	24	32.5	
Postnatal development											
Growth retardation	+	+	+	+	+	+	+	+	+	–	9/10
Mental retardation[a]	+	+	+	+	+	+	+	+	+	+	10/10
Emaciation	+	+	+	+	–	+	+	–	+	–	7/10
Physical features											
Delayed closure of fontanel[a]	+	+	+	+	+	+	+	ND	+	+	9/9
Dental enamel dysplasia[a]	+	+	+	+	+	+	ND	ND	+	+	8/8
Obstructed nasolacrimal ducts	+	+	ND	+	+	+	ND	ND	ND	–	5/6
Choanal atresia	+	+	ND	+	+	+	ND	ND	ND	–	5/6
Hyper extensible joints[a]	+	+	+	+	+	ND	+	+	ND	+	8/8
Proximal symphalangism	+	+	+	+	+	+	+	+	–	–	8/10
Interdigital webbing	+	+	+	+	+	+	+	+	–	+	9/10
Loose atrophic skin[a]	+	+	+	+	+	+	+	+	+	+	10/10
Prominent cutaneous veins[a]	+	+	+	+	+	+	+	ND	ND	+	8/8
Large floppy ears[a]	+	+	+	+	+	+	+	+	+	+	10/10
Radiographic features											
Progressive sclerosis of skull[a]	+	+	ND	+	+	+	+	+	+	+	9/9
Broad clavicles and ribs	+	+	ND	+	+	+	+	–	+	+	8/9
Short middle phalanges	+	+	+	+	+	ND	+	+	–	+	8/9
Diaphyseal undermodeling[a]	+	+	ND	+	+	+	ND	ND	+	+	7/7
Diaphyseal hyperostosis	+	+	ND	+	+	ND	+	+	–	–	6/8
Metaphyseal and epiphyseal radiolucency[a]	+	+	ND	+	+	ND	ND	ND	+	–	5/6

ND, Not described; +, present; –, absent

[a] Clinical features common to all reported cases

b). He had inter-digital webbing (Fig. 1c) and mild cubitus valgus. The skin was wrinkled and loose, and prominent veins were noted in the abdominal wall. He had mild mental retardation with a total intelligence quotient of 60. Radiological examination showed cranial hyperostosis, particularly of the skull base, a sclerotic, thick mandible, broad clavicles and ribs, and diaphyseal undermodeling of the tubular bones. Diaphyseal hyperostosis was not evident, while epimetaphyseal sclerosis or longitudinal sclerotic striation was found in the long bones. Metaphyseal equivalents of the axial skeleton showed dense sclerosis (Fig. 2a–g). Bone scintigraphy showed an increased accumulation of radiopharmaceuticals, corresponding with sclerotic regions on the roentgenograms. During follow-up to 17 years of age, he showed a stable clinical course. At 17 years of age, he had a muscular build, a height of 164.5 cm (–1.0 SD) and a head circumference of 54 cm (–1.3 SD) and weighed 56.2 kg (–0.54 SD). He underwent a surgical correction for severe anterior occlusion with prognathism. Mutation analyses for the transforming growth factor-beta1 gene (*TGFB1*) and the LDL receptor-related protein 5 gene (*LRP5*) yielded normal findings.

Discussion

We describe a boy with a disorder that is classifiable into a group of sclerosing bone dysplasias. The disorder was radiologically characterized by cranial hyperostosis, metaepiphyseal sclerosis, and diaphyseal undermodeling. In addition, it was uniquely associated with cutis laxa, enamel dysplasia, and mental retardation. According to the 'Nosology and Classification of Genetic Skeletal Disorders: 2006 revision' (Superti-Furga and Unger 2007), sclerosing bone dysplasias are subclassified into three groups: (1) neonatal osteosclerotic dysplasia group, (2) increased bone density group (without modification of bone shape), and (3) increased bone density group with metaphyseal and/or diaphyseal involvement. A few disorders in the third group, such as Camurati–Engelmann disease, craniometaphyseal dysplasia, craniodiaphyseal dysplasia, and endosteal hyperostosis, share some radiological features with the present disorder. However, the unique constellation of skeletal, skin, dental, and mental abnormalities in the present disorder excludes the possibility of these disorders. In fact, molecular analyses for *TGFB1* (the gene of Camurati–Engelmann disease) and *LRP5* (the gene of endosteal hyperostosis, Worth type) were negative.

In the differential diagnosis, LMS deserves to be discussed. The disorder is characterized by craniodiaphyseal hyperostosis and brachymesophalangy with proximal symphalangism. It is complicated by mental retardation, somatic growth failure, cutis laxa, enamel hypoplasia, and webbed fingers and toes. The manifestations of previously reported LMS patients, LMS-like patients, and the present patient are summarized in Table 1. Most findings in LMS were shared by the present disorder. However, the differences include the absence of somatic growth failure and brachymesophalangy with proximal symphalangism in the present patient. LMS patients typically exhibit diaphyseal hyperostosis and metaepiphyseal radiolucency, while the present patient had only diaphyseal undermodeling and showed metaepiphyseal sclerosis. However, the degree of diaphyseal hyperostosis is described to vary considerably among LMS patients, and some patients with metaepiphyseal sclerosis are reported in the literature (Chrzanowska et al. 1989; Spranger et al. 2002). Thus, it is tempting to assume that the present disorder may fall at the mildest end in the phenotypic continuum of LMS, suggesting that the clinical spectrum of the disorder may be broader than currently thought.

References

Braham RL (1969) Multiple congenital abnormalities with diaphyseal dysplasia (Camurati–Engelmann's syndrome). Oral Surg 27:20–26

Chrzanowska KH, Fryns JP, Krajewska M, Van den Berghe H, Wisniewski L (1989) Skeletal dysplasia syndrome with progeroid appearance, characteristic facial and limb anomalies, multiple synostoses, and distinct skeletal changes: a variant example of the Lenz–Majewski syndrome. Am J Med Genet 32:470–474

Gorlin RJ, Whitley CB (1983) Lenz–Majewski syndrome. Radiology 149:129–131

Kaye CI, Fisher DE, Esterly NB (1974) Cutis laxa, skeletal anomalies, and ambiguous genitalia. Am J Dis Child 127:115–117

Lenz W, Majewski F (1974) A generalized disorder of the connective tissues with progeria, choanal atresia, symphalangism, hypoplasia of dentine and craniodiaphysial hypostosis. Birth Defects Orig Arctic Ser 10:133–136

Macpherson RI (1974) Craniaodiaphyseal dysplasia, a disease or group of diseases? J Can Assoc Radiol 25:22–33

Majewski F (2000) Lenz–Majewski hyperostotic dwarfism: reexamination of the original patient. Am J Med Genet 93:335–338

Nishimura G, Harigaya A, Kuwashima M, Kuwashima S (1997) Craniotubular dysplasia with severe postnatal growth retardation, mental retardation, ectodermal dysplasia, and loose skin: Lenz–Majewski-like syndrome. Am J Med Genet 71:87–92

Robinow M, Johanson AJ, Smith TH (1977) The Lenz–Majewski hyperostotic dwarfism. J Pediatr 91:417–421

Saraiva JM (2000) Dysgenesis of corpus callosum in Lenz–Majewski hyperostotic dwarfism. Am J Med Genet 91:200–202

Superti-Furga A, Unger S (2007) Nosology and classification of genetic skeletal disorders: 2006 revision. Am J Med Genet 143A:1–18

Spranger JW, Brill PW, Poznanski A (2002) Bone dysplasias: an atlas of genetic disorders of skeletal development, 2nd edn. Oxford University Press, Oxford

Wattanasirichaigoon D, Visudtibhan A, Jaovisidha S, Laothamatas J, Chunharas A (2004) Expanding the phenotypic spectrum of Lenz–Majewski syndrome: facial palsy, cleft palate and hydrocephalus. Clin Dysmorph 13:137–142

REPORT

CHMP4B, a Novel Gene for Autosomal Dominant Cataracts Linked to Chromosome 20q

Alan Shiels, Thomas M. Bennett, Harry L. S. Knopf, Koki Yamada, Koh-ichiro Yoshiura, Norio Niikawa, Soomin Shim, and Phyllis I. Hanson

Cataracts are a clinically diverse and genetically heterogeneous disorder of the crystalline lens and a leading cause of visual impairment. Here we report linkage of autosomal dominant "progressive childhood posterior subcapsular" cataracts segregating in a white family to short tandem repeat (STR) markers *D20S847* (LOD score [*Z*] 5.50 at recombination fraction [θ] 0.0) and *D20S195* ($Z = 3.65$ at $\theta = 0.0$) on 20q, and identify a refined disease interval (*rs2057262*–(3.8 Mb)–*rs1291139*) by use of single-nucleotide polymorphism (SNP) markers. Mutation profiling of positional-candidate genes detected a heterozygous transversion (c.386A→T) in exon 3 of the gene for chromatin modifying protein-4B (*CHMP4B*) that was predicted to result in the nonconservative substitution of a valine residue for a phylogenetically conserved aspartic acid residue at codon 129 (p.D129V). In addition, we have detected a heterozygous transition (c.481G→A) in exon 3 of *CHMP4B* cosegregating with autosomal dominant posterior polar cataracts in a Japanese family that was predicted to result in the missense substitution of lysine for a conserved glutamic acid residue at codon 161 (p.E161K). Transfection studies of cultured cells revealed that a truncated form of recombinant D129V-CHMP4B had a different subcellular distribution than wild type and an increased capacity to inhibit release of virus-like particles from the cell surface, consistent with deleterious gain-of-function effects. These data provide the first evidence that *CHMP4B*, which encodes a key component of the endosome sorting complex required for the transport-III (ESCRT-III) system of mammalian cells, plays a vital role in the maintenance of lens transparency.

Hereditary forms of cataracts are usually diagnosed at birth (congenital), during infancy, or during childhood and are clinically important as a cause of impaired form vision development.[1] In addition to being found in >50 genetic syndromes involving other ocular defects (e.g., microphthalmia [MIM 212550]) and systemic abnormalities (e.g., galactokinase deficiency [MIM 230200]), cataracts may be inherited as an isolated lens phenotype, most frequently by autosomal dominant transmission.[2] So far, genetic linkage studies of >60 families worldwide have mapped at least 25 independent loci for clinically diverse forms of nonsyndromic cataracts on 15 human chromosomes, involving some 17 lens-abundant genes.[2] The majority of associated mutations have been identified in 10 crystallin genes (*CRYAA* [MIM 123580], *CRYAB* [MIM 123590], *CRYBB1* [MIM 600929], *CRYBB2* [MIM 123620], *CRYBB3* [MIM 123630], *CRYBA1* [MIM 123610], *CRYBA4* [MIM 123631], *CRYGC* [MIM 123680], *CRYGD* [MIM 123690], and *CRYGS* [MIM 123730]),[3–11] which encode the major "refractive" proteins of the lens. The remaining mutations have been identified in seven functionally diverse genes, including those coding for gap-junction connexin proteins (*GJA3* [MIM 121015], *GJA8* [MIM 600897]),[12,13] a heat-shock transcription factor (*HSF4* [MIM 602438]),[14] an aquaporin water channel (*MIP* [MIM 154050])[15] a claudin-like cell-junction protein (*LIM2* [MIM 154045]),[16] and intermediate-filament-like cytoskeletal proteins (*BFSP1* [MIM 603307], *BFSP2* [MIM 603212]).[17,18] In addition to the known genes, at least 10 novel genes for autosomal dominant or recessive forms of nonsyndromic cataracts remain to be identified at loci on chromosomes 1 (CCV [MIM 115665], CTPP1 [MIM 116600]), 2 (PCC [MIM 601286], CCNP [MIM 607304, MIM 115800]), 3 (CATC2 [MIM 610019]), 9 (CAAR [MIM 605749]), 15 (CCSSO [MIM 605728]), 17 (CTAA2 [MIM 601202], CCA1 [MIM 115660]), 19 (CATCN1 [MIM 609376]), and 20 (CPP3 [MIM 605387]).[19–32] Here we have fine-mapped a locus for autosomal dominant cataracts on chromosome 20q and, subsequently, have identified underlying missense mutations in the gene for chromatin modifying protein-4B (*CHMP4B* [MIM 610897]), also known as charged multivesicular body protein-4B, which has not previously been associated with human disease.

Linkage studies.—We investigated a six-generation white family from the United States (family Sk) segregating autosomal dominant progressive childhood posterior subcapsular cataracts (PCPSC) in the absence of other ocular or systemic abnormalities (fig. 1*A*). Ophthalmic records indicated that the cataracts presented in both eyes as disc-shaped posterior subcapsular opacities, progressing with age to affect the nucleus and anterior subcapsular regions of the lens (fig. 1*B*). The age at diagnosis varied from 4 to

From the Departments of Ophthalmology and Visual Sciences (A.S.; T.M.B.; H.L.S.K.), Genetics (A.S.), and Cell Biology and Physiology (S.S.; P.I.H.), Washington University School of Medicine, St. Louis, MO; and the Departments of Ophthalmology and Visual Sciences (K.Y.), and Human Genetics (K-i.Y.; N.N), Nagasaki University Graduate School of Biomedical Sciences, Nagasaki, Japan

Received March 9, 2007; accepted for publication May 9, 2007; electronically published July 27, 2007.

Address for correspondence and reprints: Dr. Alan Shiels, Department of Ophthalmology and Visual Sciences, Campus Box 8096, Washington University School of Medicine, 660 South Euclid Avenue, St. Louis, MO 63110. E-mail: shiels@vision.wustl.edu

Am. J. Hum. Genet. 2007;81:596–606. 0002-9297/2007/8103-0017$15.00
DOI: 10.1086/519980

20 years, and the age at surgery ranged from 4 to 40 years. Postsurgical corrected visual acuity varied from 20/20 to 20/200 in the better eye. Blood samples were obtained from 27 family members, and leukocyte genomic DNA was purified and quantified using standard techniques (Qiagen). Ethical approval for this study was obtained from the Washington University Human Research Protection Office, and written informed consent was provided by all participants prior to enrollment, in accordance with the tenets of the Declaration of Helsinki.

For linkage analysis, 15 affected individuals, 8 unaffected individuals, and 4 spouses from family Sk were genotyped using STR markers from the combined Généthon, Marshfield, and deCODE genetic linkage maps (National Center for Biotechnology Information [NCBI]), as described elsewhere.[33] Following exclusion of linkage to known loci for autosomal dominant cataracts on chromosomes 1–3, 10–13, 15–17, 19, 21, and 22 (table 1), we obtained significant evidence of linkage (table 2) for markers *D20S847* ($Z = 5.50$ and $\theta = 0$), *D20S195* ($Z = 3.65$ and $\theta = 0$), and *D20S870* ($Z = 3.11$ and $\theta = 0$).

Haplotype analysis detected seven recombinant individuals within the Sk pedigree (fig. 1*A*). First, two affected females, VI:4 and VI:6, were obligate recombinants, proximally at *D20S885* and distally at *D20S855*, respectively. Second, three affected females (IV:1, IV:4, and V:3) and one affected male (VI:1) were obligate recombinants distally at *D20S834*. Third, one affected female (V:3) and her affected son (VI:1) were obligate recombinants proximally at *D20S837*. However, with the exception of individual V:5 (see below), no further recombinant individuals were detected at four other intervening STR markers, suggesting that the cataract locus lay in the physical interval, *D20S837*–(4.7 Mb)–*D20S834*.

At the time of our study, individual V:5 was 17 years of age and phenotypically unaffected; however, he inherited the complete disease haplotype (fig. 1*A*), suggesting that he was either nonpenetrant or presymptomatic for cataracts. The two-point LOD scores shown in table 2 were calculated with the assumption of unaffected status for individual V:5 and 95% penetrance in family Sk; however, even when 100% penetrance was assumed, we still retained significant evidence of linkage proximally at *D20S195* ($Z_{max} = 4.31$ at $\theta_{max} = 0.04$) and distally at *D20S847* ($Z_{max} = 5.08$ at $\theta_{max} = 0.04$). Conversely, if individual V:5 developed cataracts later in life, perhaps extending the age-at-onset range in family Sk, and was included with the assumption of preaffected status and 100% penetrance, we would obtain enhanced evidence for linkage (*D20S195*, $Z_{max} = 5.12$ at $\theta_{max} = 0.0$; *D20S847*, $Z_{max} = 6.97$ at $\theta_{max} = 0.0$). However, regardless of whether individual V:5 was included or excluded, we found no evidence of linkage at other candidate genes or loci for autosomal dominant cataracts (table 1).

To further refine the disease interval, we genotyped family Sk with biallelic SNP markers (NCBI) located within the STR interval using conventional dye-terminator cycle-sequencing chemistry (Applied Biosystems). Critical affected individuals IV:1, IV:4, and V:3 were also found to be recombinant at SNP marker *rs1291139* (A/T), which lies ~0.5 Mb centromeric to *D20S834*. Similarly, critical affected individuals V:3, and VI:1 were also recombinant at marker *rs2057262* (A/C) located ~0.4 Mb telomeric to *D20S837* (fig. 1*A*). However, individual V:5 excepted, no further recombination events were detected at intervening SNP markers, indicating that the cataract locus lay in the reduced (~0.9 Mb) physical interval, *rs2057262*–(3.8 Mb)–*rs1291139* (fig. 1*C*).

Mutation analysis.—The refined SNP interval contained ~80 positional-candidate genes, none of which were obvious functional candidates for cataracts in family Sk (NCBI Map Viewer). We prioritized genes for mutation analysis of exons and intron boundaries (splice sites) on the basis of three main criteria.

1. NCBI reference sequence status, with those genes designated "reviewed" or "provisional" selected over those designated "model" or "pseudogene."
2. Evidence of expression in (fetal) eye, from the UniGene EST database.
3. Number of exons or amplicons required for coverage of the coding region, starting with smaller genes first.

Resequencing analysis of individuals IV:5, V:6, V:10, and VI:6 from the Sk pedigree (fig. 1*A*) excluded the presence of coding or splice-site mutations in eight genes (data not shown), including *EPB41L1* (MIM 602879), *E2F1* (MIM 189971), *ZNF341, PXMP4, ITGB4BP* (MIM 602912), *APBA2BP, SCAND1* (MIM 610416), and *DYNLRB1* (MIM 607167). However, resequencing of a 5-exon gene symbolized *CHMP4B* (GeneID: 128866) identified a heterozygous c.386A→T transversion in exon 3 that was not present in wild type (fig. 2*B*). This single-nucleotide change did not result in the gain or loss of a convenient restriction site; therefore, we designed allele-specific (A/T) PCR analysis to confirm that the mutant "T" allele cosegregated with affected but not unaffected members of family Sk, with the exception of individual V:5 (fig. 2*C*). Furthermore, when we tested the c.386A→T transversion as a biallelic marker, with a notional allelic frequency of 1%, in a two-point LOD score analysis of the cataract locus (table 2) we obtained further compelling evidence of linkage ($Z = 6.52$ at $\theta = 0$). In addition, we confirmed that the c.386A→T transversion was not listed in the NCBI SNP database (dbSNP), and we excluded it as a SNP in a panel of 192 normal, unrelated individuals (i.e., 384 chromosomes), using the allele-specific PCR analysis described in fig. 2*C* (data not shown). Although it is possible that an undetected mutation lay elsewhere within the disease-haplotype interval (3.8 Mb), our genotype data strongly suggested that the c.386A→T transversion in exon 3 of *CHMP4B* represented a causative mutation rather than a benign SNP in linkage disequilibrium with the cataract phenotype.

To verify that the c.386A→T transversion in *CHMP4B*

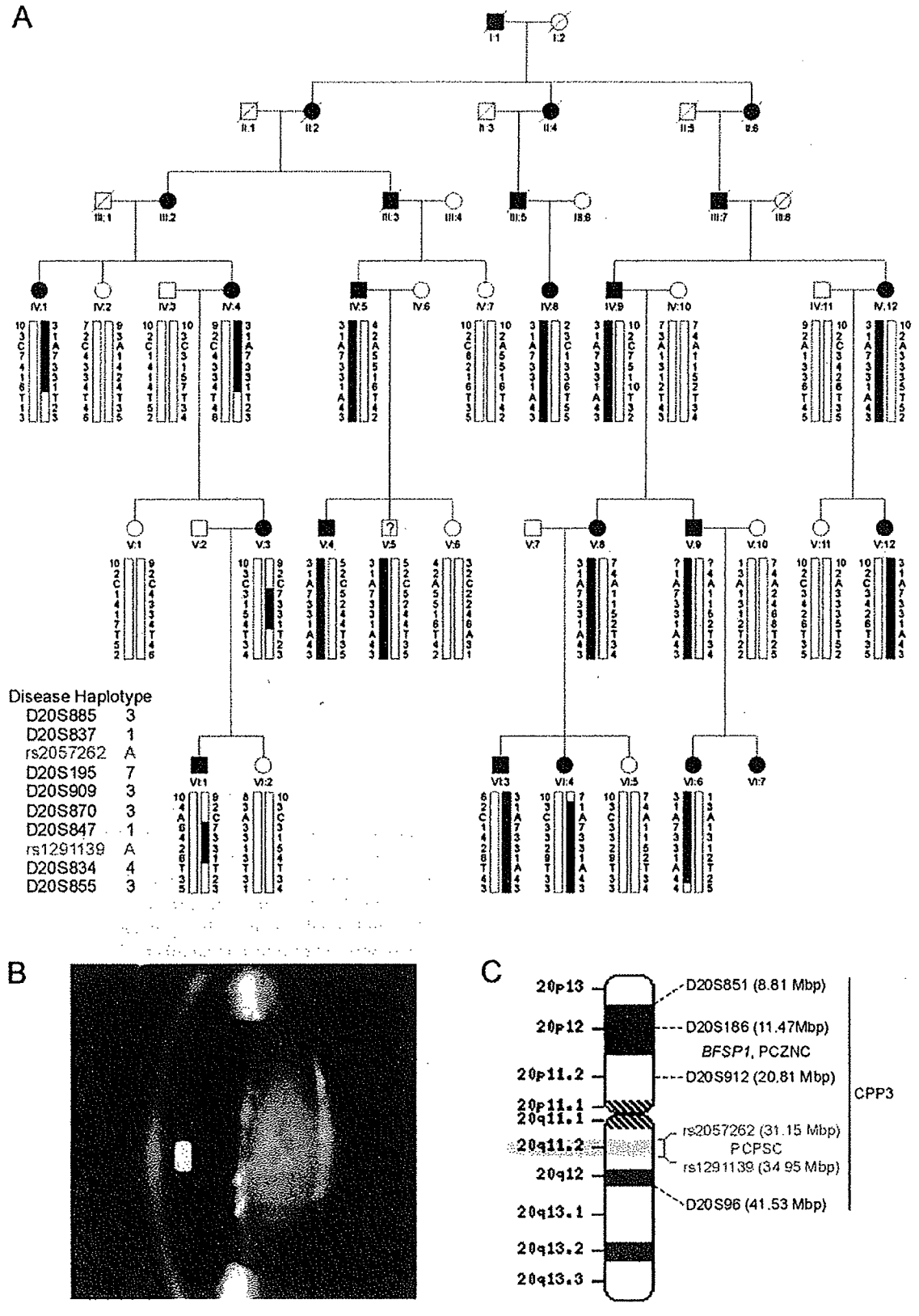
A
Disease Haplotype
D20S885 3
D20S837 1
rs2057262 A
D20S195 7
D20S909 3
D20S870 3
D20S847 1
rs1291139 A
D20S834 4
D20S855 3
B
C
20p13
20p12
20p11.2
20p11.1
20q11.1
20q11.2
20q12
20q13.1
20q13.2
20q13.3
D20S851 (8.81 Mbp)
D20S186 (11.47Mbp)
BFSP1, PCZNC
D20S912 (20.81 Mbp)
rs2057262 (31.15 Mbp)
PCPSC
rs1291139 (34.95 Mbp)
D20S96 (41.53 Mbp)
CPP3

was present at the RNA transcript level in family Sk, we performed allele-specific RT-PCR analysis of peripheral blood leukocytes (PBLs), which have been shown to express *CHMP4B*.[35] PCR primers (table 3) were designed to amplify the entire coding region of *CHMP4B* (codons 1–224) in the presence of a nested mutant (T allele) primer to detect heterozygosity in three consenting relatives, including individual V:5 (fig. 3*A*). The affected father (IV:5) and his son (V:5) were heterozygous for the wild-type (A allele) and mutant (T allele) transcripts, whereas his unaffected daughter (V:6) was homozygous for the wild-type (A allele) transcript. To gain a more accurate comparison of wild-type versus mutant CHMP4B transcript levels in PBL RNA, we then performed quantitative (q)RT-PCR with SYBR Green-1 in real time (fig. 3*B*), using a sense anchor primer paired with either a mutant (T allele) or wild-type (A allele) primer (table 3). When standardized against transcript levels for the midabundance ribosomal protein-L19 (RPL19), the ratio of wild-type to mutant CHMP4B transcripts was estimated to be 60(A):40(T), suggesting decreased expression and/or increased turnover of the mutant transcript in affected individuals. Overall, the transcript and genotype data are consistent for these individuals (fig. 1*A* and fig. 3*A*) and support the view that the clinically unaffected son (V:5) is either presymptomatic or nonpenetrant for the cataract phenotype. Moreover, the ability to amplify the intact coding region of CHMP4B transcripts from affected individuals was consistent with correct mRNA splicing, suggesting that the c.386A→T transversion, which is located near the beginning of exon 3, did not activate a cryptic splice site.[36] Finally, we also confirmed that the intact coding region of CHMP4B transcripts could be amplified from human and mouse post mortem lenses (fig. 3*C*), consistent with a functional role for CHMP4B in lens biology.

CHMP4B is cytogenetically distinct from *BFSP1* and an interval on 20p (fig. 1*C*) that was linked recently with autosomal dominant progressive congenital zonular nuclear cataract (PCZNC) segregating in a Chinese family.[32] However, *CHMP4B* is located within a much larger region spanning 20p12–20q12 that was previously linked with autosomal dominant posterior polar cataract (CPP3 [MIM 605387]) segregating in a Japanese family.[31] Like the cataracts in family Sk, CPP3 was characterized by a juvenile onset and progressive disc-shaped posterior subcapsular opacities along with some cortical opacification.[37] To investigate the possibility of allelism, we performed a similar mutation screen of *CHMP4B* in the CPP3 family and identified a heterozygous c.481G→A transition in exon 3 that was not present in wild type (fig. 4*A* and 4*B*) or in the SNP database. This single-nucleotide change removed an adjacent *Mnl*1 restriction enzyme-site, and restriction fragment length analysis confirmed that the heterozygous A allele cosegregated with affected members of the CPP3 family but was not present in unaffected relatives or our control panel (fig. 4*C* and data not shown). The identification of a second coding nucleotide change in a geographically and ethnically distinct family provided strong supporting evidence for *CHMP4B* as the causative gene for cataracts linked to 20q. In addition, the locus for lens opacity-4 (*Lop4*)[38] has been linked to a region of murine chromosome 2 that is syntenic with human 20q11.2 raising the possibility of a mouse model for the cataracts described here.

CHMP4B encodes a highly charged helical protein (~25 kDa) with N-terminal basic and C-terminal acidic halves (fig. 5*B*). The c.386A→T transversion in exon 3 occurred at the second base of codon 129 (GAT→GTT), and is predicted to result in the missense substitution of aspartic acid to valine (p.D129V) at the level of translation. Similarly, the c.481G→A transition occurred at the first base of codon 161 (GAG→AAG) of exon 3, and is predicted to translate as a missense substitution of glutamic acid to lysine (p.E161K). Cross-species alignment of the amino acid sequences for CHMP4B present in the Entrez Protein database, performed by means of ClustalW, revealed that p.D129 and p.E161 are phylogenetically conserved from yeast to man (fig. 5*C*). Moreover, the predicted p.D129V and p.E161K substitutions represented nonconservative amino acid changes, with the acidic side-group ($-CH_2COOH$) of aspartic acid replaced by the neutral, hydrophobic side-group ($-CH-C_2H_6$) of valine, and the acidic side-group ($-C_2H_4COOH$) of glutamic acid replaced by the basic side-group ($-C_4H_8NH_2$) of lysine, respectively, suggestive of functional consequences.

Functional expression studies.—Eleven CHMP genes have been identified in the human genome and, on the basis of phylogenetic analyses, have been divided into seven subfamilies, some with multiple members.[39,40] CHMP4B is one of three human orthologs of yeast Snf7/Vps32 (sucrose non-fermenting-7 or vacuolar protein sorting-32), which functions in protein sorting and transport in the endosome-lysosome pathway.[39] In the current model, CHMP4B is a core subunit of the endosomal-sorting com-

Figure 1. Autosomal dominant PCPSC in a six-generation family (Sk). *A*, Pedigree and haplotype analysis showing segregation of eight STR markers and two SNP markers on 20q, listed in descending order from the centromere. Squares and circles denote males and females, respectively. Filled symbols and bars denote affected status and haplotypes, respectively. Individual V:5 is marked with a question mark (?) to denote unknown status. Pedigree and haplotype data were managed using Cyrillic 2.1 software (FamilyGenetix). *B*, Slit-lamp image of lens from affected female V:12 (age 40 years) showing posterior subcapsular, nuclear, and anterior subcapsular opacities. *C*, Ideogram of chromosome 20, comparing the cytogenetic location of SNP markers defining the PCPSC locus in this study (*red*) with those of STR markers defining loci for CPP3 and PCZNC.[31,32]

Table 1. Two-point LOD scores (Z) Showing Exclusion of Linkage between the Autosomal Dominant Cataract Locus and STR Markers near Candidate Genes or Loci on Chromosomes Other Than 20

Marker	Z^a	θ	Chromosome	Gene/Locus
D1S243	−2.77	.10	1p36	CCV, CPP1
D1S214	−2.93	.10		
D1S2748	−2.14	.20	1p32	*FOXE3*[MIM 601094]
D1S305	−2.01	.20	1q21	*GJA8*
D2S2333	−2.35	.20	2p12	CCNP
D2S128	−3.19	.05	2q32-q36	*CRYGC, CRYGD, CRYBA2*
D2S2248	−2.75	.20		
D3S1768	−∞	.00	3p21.1-p21.3	CATC2
D3S3564	−2.34	.05		
D3S1292	−1.76	.05	3q22.1	*BFSP2*
D3S3686	−4.04	.10	3q27.2	*CRYGS*
D5S2014	−2.05	.05	5q33.1	*SPARC* [MIM 182120]
D6S1710	−2.37	.05	6q12	*GLULD1*
D9S303	−1.31	.05	9q21.31	CAAR
D9S1120	−1.28	.05		
D10S566	−2.94	.10	10q24-q25	*PITX3*[MIM 602669]
D10S1697	−3.01	.10		
D11S4154	−2.63	.05	11p13	*PAX6* [MIM 607108]
D11S4192	−2.55	.10	11q23.1	*CRYAB*
D11S1347	−3.28	.05		
D12S368	−1.94	.10	12q13.3	*MIP*
D13S175	−2.34	.05	13q11	*GJA3*
D14S1047	−2.12	.05	14q24.3	*CHX10*[MIM 142993]
D15S209	−3.14	.05	15q21-q22	CCSS0
D15S1036	−2.41	.20		
D16S412	−2.51	.10	16p12.3	*CRYM*[MIM 123740]
D16S3095	−2.99	.10	16q22.1	*HSF4*
D17S1840	−2.45	.05	17p13	CTAA2
D17S796	−2.13	.10		
D17S799	−1.79	.05	17q11.2	*CRYBA1*
D17S798	−1.18	.05		
D17S785	−2.14	.10	17q24	*GALK1*[MIM 604313]
D17S802	−1.91	.05	17q24	CCA1
D17S784	−2.67	.10		
D19S412	−2.41	.15	19q13	*LIM2*
D20S112	2.58	.08	20p11.23	*BFSP1*
D20S885	2.71	.10	20p12–20q12	CPP3
D20S847	5.08	.04		
D21S1259	−2.78	.10	21q22.3	*CRYAA*
D21S1885	−.81	.00		
D22S1154	−2.20	.15	22q11.23-q21.1	*CRYBA4, CRYBB1-4*

[a] A gene frequency of 0.0001 and a penetrance of 100% were assumed for the disease locus.

plex required for transport-III (ESCRT-III), which facilitates the biogenesis of multivesicular bodies (MVBs).[39] The only CHMP gene so far implicated in human disease is *CHMP2B* (yeast ortholog Vps2/Did4 [MIM 609512]), which has been reported to harbor mutations infrequently associated with frontotemporal dementia (FTD [MIM 600795]) and amyotropic lateral sclerosis (ALS [MIM 609512]).[41–43]

CHMP4B is found diffusely throughout the cytoplasm and/or in association with endosome-like compartments when expressed in cultured mammalian cells.[44,45] To determine the effect of the p.D129V substitution on the subcellular distribution of CHMP4B, we transfected African green monkey kidney (COS-7) cells with expression plasmids[46] encoding either wild-type or mutant forms of CHMP4B tagged at the N-terminus with the FLAG epitope. Immunofluorescence microscopy with FLAG antibody revealed that full-length wild-type (FLAG-CHMP4B) and mutant protein (FLAG-D129V-CHMP4B) were diffusely distributed (fig. 6*A* and 6*B*). At higher expression levels, both were associated with endosome-like compartments (data not shown). Overall, there were no notable differences in the subcellular localization of wild type and

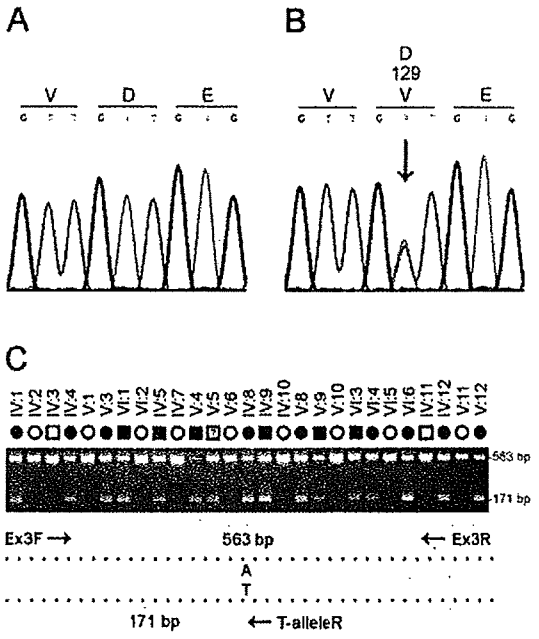

Figure 2. Mutation analysis of *CHMP4B* in family Sk. *A*, Sequence trace of the wild-type allele, showing translation of aspartic-acid (D) at codon 129 (GAT). *B*, Sequence trace of the mutant allele, showing the heterozygous c.386A→T transversion (denoted as W by the International Union of Pure and Applied Chemistry [IUPAC] code) that is predicted to result in the missense substitution of valine (GTT) for aspartate at codon 129 (p.D129V). Exons and flanking intron regions were amplified with gene-specific primers (M13-tailed) by use of the AmpliTaq PCR Master Mix in a GeneAmp 9700 thermal-cycler (Applied Biosystems). Resulting amplicons were purified using the QIAquick gel-extraction kit (Qiagen) and then direct sequenced in both directions with M13-primers and the BigDye Terminator (v.3.1) cycle sequencing kit on a 3130xl genetic analyzer running SeqScape mutation-profiling software (Applied Biosystems). *C*, Allele-specific PCR analysis using the three primers (table 3) indicated by arrows in the schematic diagram; exon 3 was amplified as above with the sense (anchor) primer located in intron 2 (Ex3F), the anti-sense primer located in intron 3 (Ex3R), and the nested mutant primer specific for the T allele in codon 129 (T-alleleR). PCR products were visualized (302 nm) on 2% agarose gels stained with ethidium bromide (EtBr). Note that only affected members of family Sk are heterozygous for the T allele (171 bp), with the exception of individual V:5, who is believed to be presymptomatic or nonpenetrant for cataracts.

Table 2. Two-Point LOD Scores (Z) for Linkage between the Cataract Locus and Markers on Chromosome 20q Listed in Physical Order (Mb) from the Short-Arm Telomere (p-tel)

Marker	Distance from p-tel		Z^a at θ =							
	cM	Mb	.00	.05	.10	.20	.30	.40	Z_{max}	θ_{max}
D20S885	39.9	17.91	−7.79	2.51	2.72	2.35	1.60	.74	2.72	.10
D20S111	49.2	29.94	−2.82	1.14	1.17	.91	.54	.19	1.18	.08
D20S837	50.7	30.73	−.81	4.15	3.98	3.18	2.14	1.01	4.15	.05
rs2057262		31.15	−4.03	−.02	.14	.16	.09	.03	.17	.15
D20S195	50.2	31.29	3.65	4.17	3.88	2.96	1.90	.87	4.20	.03
CHMP4B (A>T)		31.90	6.24	5.87	5.37	4.19	2.82	1.36	6.24	.00
D20S909	50.7	33.92	1.89	1.88	1.72	1.25	.73	.33	1.91	.02
D20S896	50.2	34.16	2.88	2.60	2.30	1.68	1.05	.46	2.88	.00
D20S870	50.7	34.16	3.11	2.93	2.63	1.94	1.23	.59	3.11	.00
D20S847	50.2	34.32	5.50	5.18	4.72	3.60	2.33	1.05	5.50	.00
rs1291139		34.95	−1.85	.99	1.10	.96	.66	.30	1.10	.11
D20S834	50.7	35.43	−1.08	2.07	1.91	1.30	.65	.19	2.07	.05
D20S607	54.9	38.23	−1.61	1.85	2.02	1.81	1.30	.66	2.03	.11
D20S855	56.0	39.08	−.29	3.26	3.19	2.58	1.71	.77	3.27	.06

NOTE.—STR marker allele frequencies used for linkage analysis were those calculated by Généthon/Marshfield/deCODE. A gene frequency of .0001 and a penetrance of 95% were assumed for the disease locus.

[a] Z values were calculated using the MLINK subprogram from the LINKAGE (5.1) package of programs.[34]

p.D129V mutant protein. In contrast, similar expression studies of a splicing mutation in *CHMP2B* underlying FTD, which resulted in truncation (36 amino acids) and miscoding (29 amino acids) at the C-terminus of the full-length protein (residues 1–213), has been associated with redistribution of CHMP2B and the formation of dysmorphic organelles of the late endosomal pathway.[41]

The p.D129V missense substitution was predicted to be located centrally in CHMP4B and to result in the net loss of a negatively charged residue (fig. 5*B*). Domain expression studies have revealed that the N-terminal half of CHMP4A (MIM 610051), an isoform of CHMP4B, is responsible for self-association into polymers and binding to membrane phospholipids.[46] To better appreciate the effects of the p.D129V substitution, we compared the subcellular localization of wild-type and mutant N-terminal fragments of CHMP4B (residues 1–150) comparable to those previously studied.[46,47] As expected, the distribution of the truncated wild-type fragment (FLAG-CHMP4B$_{1-150}$) differed from that of the full-length wild-type protein; the former appeared to be in large polymers and sometimes associated with vacuolar structures (fig. 6*C*), whereas the latter was diffuse (fig. 6*A*). Similarly, the truncated mutant fragment (FLAG-D129V-CHMP4B$_{1-150}$) differed from the full-length mutant protein; the former was concentrated on a punctate perinuclear structure (fig. 6*D*), and the latter was again diffuse (fig. 6*B*). Consistently, however, the truncated mutant fragment (fig. 6*D*) displayed a different subcellular distribution pattern from that of the truncated wild-type fragment (fig. 6*C*).

In addition to MVB formation, CHMP4B is thought to participate in the budding of a number of RNA viruses, including human immunodeficiency virus type-1 (HIV-1), from the surface of infected cells.[45] To further investigate the effect of the p.D129V substitution on CHMP4B activity in a functional assay, we compared the effect of expressing wild-type and mutant protein on release of HIV-1 virus-like-particles (VLPs). To monitor VLP production, human embryonic kidney (HEK 293T) cells were cotransfected with a plasmid encoding the HIV-1 Gag polyprotein (Pr55) and a plasmid encoding wild-type or mutant CHMP4B. HIV-1 Gag forms VLPs in the absence of other viral proteins,[48] and expression of Gag and CHMP4B

Table 3. PCR Primers for Mutation Screening and Transcript Analysis of *CHMP4B*

Primer	Location	Strand	Sequence (5′→3′)[a]
Ex1F	Exon 1	Sense	gtagtcagtggcgcgttg
Ex1R	Intron 1	Antisense	aggcgagtctgatgaaggtg
Ex2F	Intron 1	Sense	cactagaacctcaccctgtgc
Ex2R	Intron 2	Antisense	aaacaaactcaggtgctcgaa
Ex3F	Intron 2	Sense	tcacagggagtcattgcaggg
Ex3R	Intron 3	Antisense	cccaccctggaaaggtgcag
Ex3R2	Intron 3	Antisense	agggacagcctcagggtatcattt
Ex4F	Intron 3	Sense	cacagggtctggaacctggaa
Ex4R	Intron 4	Antisense	tgggcaagctcaggacacaga
Ex5F1	Intron 4	Sense	aacatgttgaacgcaccagtc
Ex5R1	Exon 5	Antisense	AGGTCATTTCAACTGCAACCA
Ex5F2	Exon 5	Sense	CGCTGACTCCACTGCTGAATCC
Ex5R2	Exon 5	Antisense	ctggaaagggtcagctcccg
StartF	Exon 1	Sense	caccATGTCGGTGTTCGGGAAGCT
EndR	Exon 5	Antisense	CATGGATCCAGCCCAGTTCTCCAA
A-alleleR	Exon 3	Antisense	CAGCAATGTCCTGCATTAACTCAT
T-alleleR	Exon 3	Antisense	CAGCAATGTCCTGCATTAACTCAA

[a] Noncoding sequence is shown in lowercase, coding sequence in uppercase.